

# Using Green-Kubo modal analysis (GKMA) and interface conductance modal analysis (ICMA) to study phonon transport with molecular dynamics

Cite as: J. Appl. Phys. **125**, 081101 (2019); <https://doi.org/10.1063/1.5081722>

Submitted: 15 November 2018 . Accepted: 01 February 2019 . Published Online: 22 February 2019

Hamid Reza Seyf, Kiarash Gordiz , Freddy DeAngelis, and Asegun Henry



View Online



Export Citation



CrossMark

## ARTICLES YOU MAY BE INTERESTED IN

[Phonon properties and thermal conductivity from first principles, lattice dynamics, and the Boltzmann transport equation](#)

Journal of Applied Physics **125**, 011101 (2019); <https://doi.org/10.1063/1.5064602>

[Interface conductance modal analysis of a crystalline Si-amorphous SiO<sub>2</sub> interface](#)

Journal of Applied Physics **125**, 135102 (2019); <https://doi.org/10.1063/1.5085328>

[Nanoscale thermal transport. II. 2003–2012](#)

Applied Physics Reviews **1**, 011305 (2014); <https://doi.org/10.1063/1.4832615>

Lock-in Amplifiers  
Find out more today



Zurich  
Instruments

# Using Green-Kubo modal analysis (GKMA) and interface conductance modal analysis (ICMA) to study phonon transport with molecular dynamics

Cite as: J. Appl. Phys. 125, 081101 (2019); doi: 10.1063/1.5081722

Submitted: 15 November 2018 · Accepted: 1 February 2019 ·

Published Online: 22 February 2019



View Online



Export Citation



CrossMark

Hamid Reza Seyf,<sup>1,a)</sup> Kiarash Gordiz,<sup>2,a)</sup>  Freddy DeAngelis,<sup>1</sup> and Asegun Henry<sup>1,2,3,b)</sup>

## AFFILIATIONS

<sup>1</sup>George W. Woodruff School of Mechanical Engineering, Georgia Institute of Technology, Atlanta, Georgia 30332, USA

<sup>2</sup>Department of Mechanical Engineering, Massachusetts Institute of Technology, Cambridge, Massachusetts 02139, USA

<sup>3</sup>School of Materials Science and Engineering, Georgia Institute of Technology, Atlanta, Georgia 30332, USA

<sup>a)</sup>**Contributions:** H. R. Seyf and K. Gordiz have equally contributed to the paper.

<sup>b)</sup>**Author to whom correspondence should be addressed:** [ase@mit.edu](mailto:ase@mit.edu)

## ABSTRACT

While current descriptions of thermal transport exist for well-ordered solids, i.e., crystal lattices, new methods are needed to describe thermal transport in systems with lack of symmetry such as structurally/compositionally disordered solids and interfaces. In this tutorial, we discuss the formalism, implementation, and application of two recently developed methods, Green-Kubo modal analysis and interface conductance modal analysis, to predict the thermal conductivity and thermal interface conductance, respectively. Specifically, these methods enable the prediction of phonon contributions to transport in crystal-line materials with any level of defects, up through fully amorphous solids, dilute to fully random alloys, molecules, nanostructures, and across interfaces involving any of these material classes—all within a single and unified perspective. This tutorial article not only describes the methods, but also provides example codes that can be used for their direct implementation. The design and functionality of the codes is also discussed in order to reduce the barrier to more extensive utilization of these approaches by others.

Published under license by AIP Publishing. <https://doi.org/10.1063/1.5081722>

## I. INTRODUCTION

In all materials, heat is conducted through the motions of atoms. In rigid bodies, the motions of atoms become localized around a fixed equilibrium site, and as a result, the motions of the atoms become vibrations. The vibrations of each atom can be viewed as a superposition of collective motions that groups of atoms make together at a single frequency, which are often termed normal modes of vibration. The amplitudes of these normal modes depend on the energy of the mode, which follows according to a quantum harmonic oscillator, occurring in integer steps of the vibrational energy  $\hbar\omega$ , where  $\hbar$  is the reduced Planck constant and  $\omega$  is the angular frequency of the vibration. Each step in vibrational energy of the mode is then

thought of as a quasi-particle termed a phonon, and the theory describing the transport of phonons is known as the phonon gas model (PGM).<sup>1–9</sup> Over the last century, PGM-based theoretical and computational techniques have successfully described the heat conduction in virtually any homogeneous crystalline solid.<sup>10–18</sup> Given its success in crystalline solids, the PGM has become the primary lens through which phonon transport is viewed across the entire spectrum of solid structures. However, when it comes to systems with broken symmetry such as random alloys, amorphous materials, individual molecules, and interfaces, no PGM-based method has shown a consistent agreement with experimental measurements. This failure primarily arises from a core assumption in the PGM,

which is that all phonons have an associated velocity. Rigorously, the assignment of a velocity presumes that all phonons resemble plane waves with well-defined wave vectors, which then enables the identification of a group velocity for a group of modes that have been added together to form a wave packet. However, in structurally or compositionally disordered solids as well as solid-solid interfaces, due to the break in symmetry/homogeneity, the character of vibrational modes drastically changes and can be very different from the conventional traveling plane wave picture of a phonon.<sup>19</sup> Therefore, to correctly describe the heat conduction in solids with broken symmetry, different techniques are needed that are not based on the inherent assumptions in the PGM. Recently, several approaches have been proposed to directly assess a mode's thermal conductivity (TC)<sup>4,20–22</sup> and thermal interface conductance (TIC)<sup>3,23–26</sup> contribution, without any invocation of the PGM, in particular, Green-Kubo modal analysis (GKMA)<sup>4</sup> and interface conductance modal analysis (ICMA)<sup>3,23</sup> to predict TC and TIC between any two groups of atoms, respectively. A detailed discussion regarding the application of these two formalisms is the focus of this tutorial article. We will discuss how these methods are formulated and how they can be integrated into the freely available existing computational platforms to predict the contributions of phonons to transport coefficients regardless of their mode shape/character. Specifically, the GKMA and ICMA methods enable the prediction of phonon contributions to transport in crystalline with any level of defects, up through fully amorphous solids, dilute to fully random alloys, molecules, nanostructures, and across interfaces involving any of these material classes—all within a single and unified perspective.

The remainder of this article is organized as follows: a correlation-based theory for phonon transport based on the Green Kubo formula, i.e., GKMA, is introduced in Sec. II, then it is applied to calculate the TC of well-ordered crystalline materials, amorphous solids, and random alloys as example case-studies. In Sec. III, we introduce the ICMA method, which is a correlation-based technique to describe the interfacial heat transfer. In Sec. III, we also discuss three enlightening insights into the interfacial heat conduction that arise from ICMA. The correct implementation and computational considerations of GKMA and ICMA formalisms will be discussed in Secs. II and III, respectively, as well. We note that, since this article is a tutorial and not a review, it is not meant to be exhaustive. Interested readers are directed to read other papers in the literature<sup>3–7,23,27–35</sup> for more in-depth studies of the associated physics. Here, we give references whenever relevant, but limit them to selected references that are most directly connected to the subjects of interest.

## II. GREEK-KUBO MODAL ANALYSIS

### A. Green Kubo (GK) method

GKMA is an approach<sup>4</sup> based on a combination of molecular dynamics (MD) and lattice dynamics (LD). GKMA is based

on the Green-Kubo (GK) method, which is an approach that can be used to compute the TC of any phase of matter, i.e., solids, liquids, gases, etc. It is based on fluctuation-dissipation theorem and one can use equilibrium MD simulations, as opposed to non-equilibrium, to evaluate the volume averaged heat current for a group of atoms. In the GK approach, the TC is related to the equilibrium fluctuations in the heat current, via its autocorrelation function

$$\kappa_{\alpha\beta} = \frac{V}{k_b T^2} \int \langle \mathbf{Q}_\alpha(t+t') \mathbf{Q}_\beta(t) \rangle dt', \quad (1)$$

where  $\langle \mathbf{Q}_\alpha(t+t') \mathbf{Q}_\beta(t) \rangle$  is the heat flux autocorrelation function (HFAC),  $V$  is the system volume,  $k_b$  is the Boltzmann constant,  $T$  is the system temperature,  $\mathbf{Q}$  is the heat current vector,  $\alpha$  and  $\beta$  denote the components of thermal conductive tensor, and the angular brackets denote an ensemble average, or, in the case of an ergodic system, it can be replaced with the time average.<sup>1</sup>

An important issue associated with the GK method is the precise definition of the heat current. Hardy<sup>36</sup> has derived a heat current operator that uses a spatial weighting function to describe the local energy density as a continuous function. Hardy's result is valid for any system where the energy is expressed in the form

$$E = \sum_i \frac{1}{2} m_i v_i^2 + \Phi_i, \quad (2)$$

where  $E$  is the kinetic and potential energy,  $\Phi_i$  is the potential energy associated with a single atom,  $m_i$  is the mass of atom, and  $v_i$  is the velocity of the atom. Hardy's result for the heat flux operator is expressed as

$$\mathbf{Q} = \frac{1}{V} \sum_i \left[ E_i \cdot \mathbf{v}_i + \sum_j (-\nabla_{\mathbf{r}_i} \Phi_i \cdot \mathbf{v}_i) \cdot \mathbf{r}_{ij} \right], \quad (3)$$

where  $r_{ij}$  is the distance between atoms  $i$  and  $j$ . Hardy's result is general and can be applied to any empirical potential, provided the energy can be written in terms of individual atoms. Equation (3) has two physically meaningful terms that correspond to the two mechanisms that carry heat in all phases of matter. The first term, often called the convective or diffusion term, dominates in gases where energy is transported through the kinetic energy of the constituent molecules.<sup>36</sup> In solids and liquids, because the forces are large and atoms are more so constrained to their local environment the second term in Eq. (3) dominates.

The correlation of the heat current in Eq. (1) measures how similar the heat current is at some time  $t$  and another later time  $t'$ . The more similar the heat current fluctuations are, the longer the memory of the initial perturbations the system experienced, and as a result, the inner product between the two is larger. This leads to more correlation and consequently higher the TC. Thus, in low TC solids, the correlation is usually short-lived (i.e., a few picoseconds), while in high TC materials, the

fluctuations remain correlated for longer times (i.e., tens to hundreds of picoseconds) as the memory of the earlier state dissipates more slowly.

Since the GK formula can be evaluated using MD simulations, all degrees of anharmonicity, i.e., 3-phonon, 4-phonon up to N-phonon interactions are naturally included in the heat current, therefore TC. Furthermore, GK can be used to study defects, disorder, and finite size effect explicitly, as opposed to treating them as perturbations to some homogeneous and infinitely large system. In this way, one can evaluate the dynamics of an actual and specific configuration of atoms, rather than relying on effective medium and perturbation schemes. Instead, one can evaluate effects like disorder by statistically sampling different configurations that have the same descriptor of interest, i.e., the same defect density or the same interface roughness. Finally, since the GK formula does not cast TC in terms of phonons directly, but instead in terms of atoms, there is no utilization of quantities such as group velocity to calculate the TC. In fact, it makes no assumptions about the phase of matter, and as a result, this approach can be used to predict TC of materials with broken symmetry such as non-crystalline solids, random alloys, and molecules. Although GK has several advantages, it is not able to provide information on the contributions of individual vibrational modes to the TC. This is because it is formulated completely independent of the notion of a phonon, as it is equally valid for liquids and gasses, where phonons are not even a well-defined phenomenon. Nonetheless, for solids/rigid bodies, phonons exist, and in Sec. II B, we explain how GKMA can be used to extract information about phonons from the GK framework.

## B. GKMA formulation

Consider an arbitrary object with N atoms vibrating around their equilibrium positions. The object can have any internally inhomogeneous structure and/or composition and need not be periodic in any sense whatsoever. For such a system, using a harmonic or anharmonic LD calculation, one can obtain 3N collective modes of vibration.<sup>37</sup> The most general approach that would be applicable to both crystalline and non-crystalline materials is to perform the LD

calculations on the entire supercell ( $k = 0$ , also known as the  $\Gamma$ -point) as if it were a single unit cell. With the 3N modes determined, one can then use the individual polarization vectors for each atom in a mode as a basis set for projecting the anharmonic trajectory from MD. Toward this end, we first show transformation from individual atom coordinates to normal mode coordinates, where the normal mode coordinates of position  $X_n(t)$  and velocity  $\dot{X}_n(t)$  for mode  $n$  can be written as

$$X_n(t) = \sum_j \sqrt{m_j} \mathbf{e}_{j,n}^* \cdot \mathbf{x}_j(t), \quad (4)$$

$$\dot{X}_n(t) = \sum_j \sqrt{m_j} \mathbf{e}_{j,n}^* \cdot \dot{\mathbf{x}}_j(t), \quad (5)$$

where  $\mathbf{e}_{j,n}$  is the eigenvector that gives the magnitude and direction of motion for atom  $j$  in mode  $n$ ,  $*$  represents the complex conjugate,  $m_j$  is the mass of atom  $j$ , while  $\mathbf{x}_j$  and  $\dot{\mathbf{x}}_j$  are the displacement and velocity vectors of atom  $j$  in the system, which can also be obtained from the reverse transformation that starts with known normal mode coordinates,

$$\mathbf{x}_j(t) = \sum_n \mathbf{x}_{j,n}(t) = \frac{1}{\sqrt{m_j}} \sum_n \mathbf{e}_{j,n} \cdot X_n(t), \quad (6)$$

$$\dot{\mathbf{x}}_j(t) = \sum_n \dot{\mathbf{x}}_{j,n}(t) = \frac{1}{\sqrt{m_j}} \sum_n \mathbf{e}_{j,n} \cdot \dot{X}_n(t). \quad (7)$$

Equations (6) and (7) essentially state that at every instant, every atom's position and velocity are a superposition of individual contributions from all normal modes of vibration in the system. These individual contributions are proportional to  $X_n(t)$  and its time derivative  $\dot{X}_n(t)$ . Recognizing the meaning of this forward and backward transformation, one can then substitute the modal contributions to the velocity of each atom into the heat flux operator derived by Hardy<sup>36</sup> [Eq. (3)], to obtain each mode's contribution to the volume averaged heat flux at each time step in an equilibrium molecular dynamics (EMD) simulation,

$$\mathbf{Q} = \sum_n^{3N} \mathbf{Q}_n(t) = \sum_n^{3N} \frac{1}{V} \sum_i \left\{ E_i \dot{\mathbf{x}}_{i,n}(t) + \sum_j [-\nabla_{\mathbf{r}_i} \Phi_j \cdot \dot{\mathbf{x}}_{i,n}(t)] \mathbf{r}_{ij} \right\} = \sum_n^{3N} \frac{1}{V} \sum_i \left\{ E_i \left[ \frac{1}{m_i^{\frac{1}{2}}} \mathbf{e}_{i,n} \dot{X}_n(t) \right] + \sum_j \left[ -\nabla_{\mathbf{r}_i} \Phi_j \cdot \left( \frac{1}{m_i^{\frac{1}{2}}} \mathbf{e}_{i,n} \dot{X}_n(t) \right) \right] \mathbf{r}_{ij} \right\}. \quad (8)$$

This then yields the individual modal contributions to heat flux as

$$\mathbf{Q}_n(t) = \frac{1}{V} \sum_i \left\{ E_i \left[ \frac{1}{m_i^{\frac{1}{2}}} \mathbf{e}_{i,n} \dot{X}_n(t) \right] + \sum_j \left[ -\nabla_{\mathbf{r}_i} \Phi_j \cdot \left( \frac{1}{m_i^{\frac{1}{2}}} \mathbf{e}_{i,n} \dot{X}_n(t) \right) \right] \mathbf{r}_{ij} \right\}, \quad (9)$$

where  $\mathbf{Q}(t) = \sum_n \mathbf{Q}_n(t)$ . By substituting Eq. (9) into Eq. (1), one can obtain the contribution of mode  $n$  in total TC,

$$\kappa_{\alpha\beta,n} = \frac{V}{k_b T^2} \int \langle \mathbf{Q}_{\alpha,n}(t+t') \mathbf{Q}_{\beta,n}(t) \rangle dt'. \quad (10)$$

If one sorts the vibrational modes ( $n$ ) based on their frequencies, the modal contributions to TC can be represented in the form of the frequency-based TC accumulation function. It is important to emphasize here that having the full mode level detail is powerful because one can resort the contributions of the different modes according to any descriptor as desired. For example, one could compute the relaxation times or mean free paths (MFPs) associated with different modes in a crystal, to then determine the accumulation as a function of MFPs.<sup>4</sup> Alternatively, one could sort the modal contributions by another descriptor, such as the phase quotient<sup>38</sup> or any other descriptor that can be well defined for all the modes in a given structure. Furthermore, one can also substitute the summation of modal contributions to the heat flux in both places of the heat flux autocorrelation to obtain the TC as a double summation over individual mode-mode heat flux cross-correlation functions,

$$\begin{aligned} \kappa_{\alpha\beta} &= \frac{V}{k_b T^2} \int \left\langle \sum_n \mathbf{Q}_{\alpha,n}(t+t') \sum_{n'} \mathbf{Q}_{\beta,n'}(t) \right\rangle dt' \\ &= \frac{V}{k_b T^2} \sum_{n,n'} \int \langle \mathbf{Q}_{\alpha,n}(t+t') \mathbf{Q}_{\beta,n'}(t) \rangle dt'. \end{aligned} \quad (11)$$

This allows the TC contribution due to correlation between pairs of modes, which can be calculated as

$$\kappa_{\alpha\beta,nn'} = \frac{V}{k_b T^2} \int \langle \mathbf{Q}_{\alpha,n}(t+t') \mathbf{Q}_{\beta,n'}(t) \rangle dt'. \quad (12)$$

Equation (10) allows one to obtain each mode's contribution to the total TC while Eq. (12) can be used to examine how the correlation between pairs of modes contributes to TC. Here, it should be noted that the correlation between modes  $n$  and  $n'$  contains all the levels of phonon-phonon interactions and should not be interpreted as two-phonon interactions. This is because the modal heat fluxes calculated from the interatomic forces, distances, and atomic positions [as shown in Eq. (9)] which include all the phonon interaction information for solids. In PGM paradigm, the scattering events create or annihilate phonons,<sup>1,9</sup> but this physical picture is disjoint with what occurs in a MD simulation. In a MD simulation, the phonon interactions occur continuously, as there is no sudden scattering

event or discrete change in amplitude. If one were to, for example, generate wave packet, all the phonons participating in the wave packet oscillate continuously together to contribute to the heat flow. During these oscillations, the different modes are continually interacting, and the energy in the modes gradually couples to other modes which break up the collective oscillation over a time scale equivalent to the relaxation time. Thus, the MD perspective is that phonons continuously interact and wave packets made from groups of phonons gradually dissipate their energy via attenuation, which differs from the particle based physical picture consisting of discrete scattering events.

In concept, PGM based methods attempt to measure the time/distance between dephasing and the loss of correlation for wave packets, while GKMA measures the correlation itself. In the GKMA paradigm, the correlation pair of mode  $n$  and  $n'$  does not translate to a two-phonon interaction, but instead it includes all 3-phonon, 4-phonon, and higher order scattering related information. It has not yet been proven, but it should be noted that by representing the potential energy as a Taylor expansion, one might be able to extract two-phonon, three-phonon, and  $N$ -phonon scattering related information. This is because the heat flux and TC would become separable into 2nd order, 3rd order, and higher contributions. However, from the GKMA perspective, all that matters is how long two phonons ( $n$  and  $n'$ ) stay correlated, which is proportional to their corresponding contribution to TC. The longer they remain correlated, the more they contribute to the net heat flow.

In the GKMA formalism, the atomic velocities are decomposed to obtain the modal contributions to the TC. Alternatively, one might prefer to obtain modal components by decomposing the force vector  $-\nabla_{\mathbf{r}_i} \Phi_i$ , or position vector  $\mathbf{r}_{ij}$  instead. To decompose the heat current based on force, one can write the force term in Eq. (3) as a scalar modal force amplitude

$$F_{i,n} = \sum_j \sqrt{m_j} \mathbf{e}_{j,n}^* \cdot (-\nabla_{\mathbf{r}_i} \Phi_j). \quad (13)$$

Similar to velocity, the force vector needed in the heat current should then be obtained by summation of the modal force amplitudes, multiplied by each atom's polarization vector,

$$\begin{aligned} -\nabla_{\mathbf{r}_i} \Phi_j &= \sum_n \mathbf{f}_n = \sum_n \frac{1}{\sqrt{m_j}} \mathbf{e}_{j,n} \cdot F_{i,n} \\ &= \sum_n \left[ \frac{1}{\sqrt{m_j}} \mathbf{e}_{j,n} \cdot \sum_j \sqrt{m_j} \mathbf{e}_{j,n}^* (-\nabla_{\mathbf{r}_i} \Phi_j) \right]. \end{aligned} \quad (14)$$

To obtain each mode's contribution to the volume averaged heat flux at each time step in an EMD simulation, one can substitute Eq. (14) into the second term of Eq. (3)

$$\mathbf{Q} = \sum_n \mathbf{Q}_n = \sum_n \frac{1}{V} \sum_i \left[ E_i \cdot \mathbf{v}_i + \sum_j (\mathbf{f}_n \cdot \dot{\mathbf{x}}_i) \mathbf{r}_{ij} \right] = \sum_n \frac{1}{V} \sum_i \left[ E_i \cdot \mathbf{v}_i + \sum_j \left( \left\{ \frac{1}{\sqrt{m_j}} \mathbf{e}_{j,n} \left[ \sum_{j'} \sqrt{m_{j'}} \mathbf{e}_{j',n}^* (-\nabla_{\mathbf{r}_i} \Phi_{j'}) \right] \right\} \cdot \dot{\mathbf{x}}_i \right) \mathbf{r}_{ij} \right]. \quad (15)$$

Although this can be accomplished mathematically, an important seemingly subtle problem arises, which was encountered when attempting to implement a force based modal decomposition. The problem with force decomposition is that it cannot be done for systems employing periodic boundary conditions, which is most common in simulations that approach the limiting behavior of a bulk material or have some macroscopic dimension. The issue with periodic images is the fact that the corresponding  $\mathbf{r}_{ij}$  that must be used for each term in the decomposition is different for an atom in the cell versus a periodic image. The problem then arises from the fact that the periodic image of an atom has exactly the same polarization vector as the atom within the supercell. Therefore, when one multiplies the modal force amplitude in Eq. (14) by the atom's polarization vector, one does not obtain the force between atom  $i$  and  $j$ , but instead the sum of force terms between  $i$  and  $j$ , including all periodic images of  $j$ . This then becomes problematic, because one cannot obtain the force terms for each individual instance/image of  $j$  and therefore one cannot multiply each term by the appropriate  $\mathbf{r}_{ij}$  for each respective instance/image. This issue essentially shows that force decomposition would rely on every atom in the system having a different polarization vector so that one can properly map the force contributions to the corresponding values of  $\mathbf{r}_{ij}$ . Thus, the central problem with using force as a basis for decomposition is the inability to properly map the force components to the correct atoms, since the summation in Eq. (15) simply returns the sum of all forces between atom  $i$  and all atoms with the polarization vector  $\mathbf{e}_j$ . Clearly, this is problematic for periodic boundary conditions, but it is also problematic for structures where the eigenvectors themselves are periodic, which is generally the case for sinusoidally modulated/propagating modes. When Eq. (15) is evaluated for crystal, one would not be able to properly separate interactions between individual atoms and periodic instances of the same basis atom in different unit cells. This issue is therefore problematic in general for systems with symmetry, such as crystalline solids. Thus, although we identified the issue in the context of assessing periodic boundary conditions, the issue is more general and is associated with periodicity in the polarization vectors and the decomposition of the heat current based on force is problematic.

Decomposing the heat current based on position by projecting  $\mathbf{r}_{ij}$  onto the polarization vectors is also problematic based on the following simple thought experiment. Consider the system at the following state, which is a common initial condition, used in many MD simulations, whereby all atoms are at their equilibrium sites, but have initial velocities. In this state, the heat current would be non-zero because the velocities are nonzero and can be asymmetric. However, if one were to have decomposed the heat current based on the displacements, in this state, all modal contributions will become equal to zero because the displacements are zero. This is because when one expands the difference in atom positions, there are two components to the vector  $[\mathbf{r}_{ij} = \mathbf{r}_{i0} + \mathbf{u}_i - (\mathbf{r}_{j0} + \mathbf{u}_j) = \mathbf{r}_{i0} - \mathbf{r}_{j0} + \mathbf{u}_i - \mathbf{u}_j]$ . The modal decomposition would arise from each atom's relative

displacement from equilibrium (e.g., the  $\mathbf{u}_i - \mathbf{u}_j$  term) and in the aforementioned state, all modal contributions would be zero since every atom would be located at its equilibrium position  $\mathbf{r}_{i0}$ . As a result, the entire heat current would arise from the term associated with  $\mathbf{r}_{i0} - \mathbf{r}_{j0}$ , which is static and only gains time dependence through its multiplication with the force and velocity terms. Therefore, the problem with such a modal decomposition is the fact that no matter what modes are excited at the proposed initial state, decomposing based on position would yield the same modal contributions (e.g., all zero), which is clearly incorrect. In conclusion, the decomposition based on velocity has been used in GKMA and ICMA, because it can be implemented in general, and the most obvious alternative decompositions are incorrect/problematic.

### C. Quantum correction

Since GKMA can provide frequency dependent TC, one can apply a quantum correction to the classical MD GKMA results at different temperatures to map classically predicted TC onto a corresponding quantum corrected value. The underlying assumption in doing so is that only the quantum effect on the specific heat must be accounted for. Turney *et al.*<sup>39</sup> have shown that for crystalline materials there are two quantum effects: (i) quantum effects on the scattering rate due to incorrect mode-mode occupations and (ii) quantum effects on the heat capacity. The first is important, as one could envision that in the limit that only a single mode is excited in the system, the time it takes for it to couple to other modes and relax toward equipartition is a strong function of the amplitudes of other modes. Thus, when other modes are simultaneously excited, it affects the rate at which mode-mode interactions occur. It has been shown that for crystalline solids this effect is critical,<sup>39</sup> and because classical MD trajectories do not yield the correct quantum mode amplitudes observed at low temperatures, MD incorrectly predicts higher scattering rates. However, even though this issue is important for crystalline solids, in situations where the phonon-phonon scattering processes are not the primary mechanism governing the low frequency mode TC contributions, one would imagine that the error associated with incorrect mode-mode occupations at low temperatures could become negligible. For instance, in low dimensional (e.g., nanoparticles and nanowires) systems where the majority of the low frequency phonon contributions are limited by scattering with the boundaries, the net relaxation time for most modes is dictated by the system dimensions and not the detailed mode-mode interactions, which require the mode occupations to be correct. This is especially the case for the low frequency modes which are the only modes that remain excited at low temperatures. As a result, in such a situation, one would imagine that application of a quantum heat capacity correction could still lead to good predictions/agreement with experimental data.

Using GKMA, one can calculate the TC of individual modes. However, a few temperature dependent corrections

are needed to accurately predict the TC. Due to its classical nature, MD results in a constant heat capacity with respect to temperature, since every mode is equally excited at all temperatures. However, once each individual mode's TC is obtained, one can easily apply a quantum specific heat correction, which extends the MD based predictions to essentially any temperature. To obtain an accurate temperature dependence TC, Lv and Henry<sup>6</sup> used the following expression:

$$\kappa(T) = \sum_n f_Q[\omega_n(T), T] f_{k,n}(T), \quad (16)$$

where the index  $n$  denotes the  $n^{\text{th}}$  vibrational mode in the system. Equation (16) includes three explicit functions of temperature, namely,  $f_Q$ ,  $f_k$ , and  $\omega$ . In this equation, the function  $f_Q$  represents the ratio of quantum to classical specific heat for mode  $n$ , which has frequency  $\omega$  at temperature  $T$  and is unit-less. The function  $f_k$  represents the GKMA derived modal contributions to TC (e.g., it has the units of TC), obtained from MD simulations conducted at the simulation temperature of  $T$ . The function  $\omega$  represents the phonon frequency of mode  $n$ , which itself might also exhibit some temperature dependence.

The quantum to classical specific heat ratio ( $f_Q$ ) is the most important source of temperature dependence. It restricts the contributions of the high frequency modes at low temperatures and modulates the MD derived TC contributions determined from the GKMA method. The quantum expression of volumetric specific heat, based on Bose-Einstein statistics, is given by

$$C_q(\omega, T) = \frac{k_B x^2}{V} \frac{e^x}{(e^x - 1)^2}; \quad x = \frac{h\omega}{k_B T} \quad (17)$$

and the classical volumetric specific heat is given by  $C_c = \frac{k_B}{V}$ . Thus, the quantum heat capacity correction factor which is the ratio of  $C_q$  and  $C_c$  is

$$f_Q(\omega, T) = \frac{C_q(\omega, T)}{C_c} = \frac{x^2 e^x}{(e^x - 1)^2}. \quad (18)$$

The second source of temperature dependence enters through the GKMA derived TC contributions ( $f_k$ ). As temperature changes, the modal interactions change, and the contributions of different modes are inherently temperature dependent via the anharmonic nature of the interactions. However, unlike the quantum specific heat correction, which is a continuous function of temperature, MD simulations are run at discrete temperatures. To then generate a piece-wise continuous function for TC vs. temperature, one can interpolate the data for  $f_k$  at discrete values of temperature. Here, one can use the data at a few initial temperatures and determine by inspection, what temperature ranges may require additional simulations to improve the resolution of the temperature dependence, e.g., in temperature ranges where the contributions change more rapidly. This is because it is advantageous to minimize

the number of temperatures needed for  $f_k$  to minimize computational expense. Suppose for a given material, we calculated the frequency dependent TC at 3 temperatures, i.e.,  $\kappa_{T_1}$ ,  $\kappa_{T_2}$ , and  $\kappa_{T_3}$ . Since in the classical MD simulations, all of the modes are excited, one can determine the mode diffusivity from the mode TC by dividing it by the classical specific heat, i.e.,  $D_T = \frac{\kappa_T}{C_c}$ . For the intermediate temperatures, one can linearly interpolate the mode diffusivity using the two temperature GKMA results for each individual mode diffusivity

$$D_T = \frac{D_{T_1}(T_2 - T) + D_{T_2}(T - T_1)}{(T_2 - T_1)}. \quad (19)$$

After interpolation, one obtains the mode diffusivity and multiplies by the quantum corrected specific heat using Bose-Einstein statistics to yield the TC at a given temperature.

Finally, the phonon frequencies ( $\omega$ ) can slightly change with temperature, due to anharmonicity and thermal expansion.<sup>40</sup> If the GKMA simulations are performed at a constant volume, thermal expansion does not play a role, but anharmonic effects can still cause the mode frequencies to change. The extent of the frequency shift as a function of temperature can be determined by interpolation of the data at discrete temperatures, using the peak frequency obtained from a Fourier transform of the mode amplitudes.

Using GKMA and temperature dependent corrections, one can accurately calculate the temperature dependent TC. It should be noted that in Eq. (16), the quantum effect is included once for every individual mode. After calculating one mode correlations with all other modes, the specific heat is corrected for that mode. Using this method, we consider whether one mode is activated or not at a specific temperature based upon its specific heat ratio. However, Eq. (20) does not consider whether the other modes with which they are correlated are excited from ground state or not at the specific temperature. However, this can be remedied by applying the quantum correction to both modes in each pair. The idea here is to use the square root of each mode's quantum correction so that when multiplied a combined correction with the correct units is obtained via

$$\kappa_{\alpha\beta,nn'} = \frac{V}{k_b T^2} \int_0^\infty \left\langle \left( \mathbf{Q}_{\alpha,n}(t) \sqrt{\frac{C_q(\omega_n, T)}{C_c}} \right) \left( \mathbf{Q}_{\beta,n'}(0) \sqrt{\frac{C_q(\omega_{n'}, T)}{C_c}} \right) \right\rangle dt, \quad (20)$$

where  $n$  and  $n'$  represent two modes,  $Q$  is the heat current for a mode,  $C_q$  is the quantum specific heat from Bose Einstein statistics,  $C_c$  is the classical specific heat, and  $\omega$  is the frequency of the mode. It should be noted that the choice of using the product of square roots of each mode's heat capacity is not arbitrary, but instead motivated by a derivation given in a prior work by Henry and Chen.<sup>33</sup> In their derivation, they represented the heat flux according to the PGM and

merged it with the GK approach by substituting the phonon heat flow for the volume averaged heat flow derived by Hardy. The result of that derivation ultimately led to an expression that contained the square root of one phonon's quantum heat capacity multiplied by the square root of another phonon's quantum heat capacity. The remainder of the expression contained quantities that were related to the phonon-phonon interactions, but the main point of relevance here, is that a quantum version of the GK expression that expresses the TC of phonons, is proportional to the product of square roots of the two modes interacting. This is the motivation behind the form of Eq. (20), which can be applied to the 2D correlation maps. This second approach is not equivalent to the expression in Eq. (16) and will yield different total TC values, but this approach is possibly better in the sense that it may, to some extent, account for the second quantum effect on the scattering rate due to incorrect mode-mode occupations.

#### D. Implementation and computational cost

The computational time required for a GKMA calculation can be a large addition to a basic MD simulation. One approach is to use a MD code such as the Large-scale Atomic/Molecular Massively Parallel Simulator (LAMMPS)<sup>41</sup> to perform the MD simulations, outputting the atomic trajectories, system energy, and forces on the atoms at every time step, and writing separate programs to post-process those recorded trajectories to calculate the modal heat flux values using a scripting language like Python with the NumPy module.<sup>42</sup> However, this approach would be much more expensive than calculating the mode level heat fluxes concurrently with the MD force evaluations. Therefore, a more efficient approach is to calculate the modal heat fluxes from within the MD code and periodically write them to file, and then use post processing to calculate the auto-correlations needed to determine the modal TCs. In this section, the implementation of GKMA in the open source package LAMMPS<sup>41</sup> and the reduction of the computational cost will be discussed. The same procedure can be applied to other MD engines as well, but an example and general implementation that can be used for any potential already coded in LAMMPS has already been developed by modifying the “compute heat/flux” command in LAMMPS, which will be discussed in more detail later.

It is important to note that eigenvectors of the supercell should be calculated before computing heat fluxes. External tools are available to calculate phonon frequencies and eigenvectors for the supercell of interest. Several open-source codes, such as General Utility Lattice Program (GULP),<sup>43</sup> PHONOPY,<sup>44</sup> and ALAMODE,<sup>15</sup> exist to calculate these quantities, which are a function of the equilibrium positions of the atoms in the supercell. To determine the equilibrium positions, a constant pressure relaxation via, e.g., LAMMPS<sup>41</sup> or GULP<sup>43</sup> is necessary before computing the dynamical matrix. For the examples presented in this tutorial, we used GULP to minimize the supercells and to calculate phonon frequencies

and eigenvectors. Once the modal heat fluxes are obtained, the contribution of each mode to the TC can be calculated from the correlation functions of the heat flux, after which quantum correction is applied to the modal TCs.

We have written a compute *gkma* command to perform GKMA calculations in LAMMPS. This compute command is based on a modified version of LAMMPS's compute *heat/flux* command. Whereas compute *heat/flux* allows one to determine the total heat flux in the x, y, and z directions in a material, compute *gkma* has been written such that it calculates modal contributions to heat flux [ $Q_n$  in Eq. (9)]. A description of compute *gkma* and an example implementation follow.

All modifications we have made to LAMMPS's compute *heat/flux* command are bracketed with comments “GKMA-beg-#” and “GKMA-end-#,” where # is a number used to refer in this text to one of the three specific blocks of edited code.

The first modification to compute *heat/flux* (block 1 in compute *gkma*) simply allocates additional variables, or in a few cases, it changes a variable type during allocation. The first substantive change to the code (block 2) reads information about the system eigenvectors, which are stored in the variables *eigx*, *eigy*, and *eigz*. The code is designed to read information from the *eigvector.eig* file produced by the General Utility Lattice Program (GULP). This file should be located in the same directory as all the other LAMMPS input files. If the user has obtained eigenvector information from another program, the eigenvector file should be modified to follow GULP's *eigvector.eig* format exactly, including blank lines, etc. Alternatively, the user can modify compute *gkma* to read an eigenvector file that has been formatted differently. Regardless, the user should ensure they have allocated enough memory to store all information from the eigenvector file, which can be a significant memory requirement for larger systems, due to the  $N^2$  scaling of eigenvector information.

The other significant change implemented in compute *gkma* can be found in block 3. There are first several minor alterations made to the code to initialize additional variables, after which the code calculates modal contributions to the heat flux. First, Eq. (5) is used to determine modal velocities, *xdotx*, *xdoty*, and *xdotz*. The subsequent *for loop* then calculates modal heat fluxes, by first implementing Eq. (7) to decompose atomic velocities into modal atomic velocities, *vx*, *vy*, and *vz*, then calculating the contribution of those modal velocities to the heat flux, *jcx*, *jcy*, *jcZ*, *jvx*, *jvy*, and *jvz* via Eq. (9). These six heat flux quantities are the modally decomposed versions of the identically-named quantities found in compute *heat/flux*. The quantities *vsum* and *actv* are for debugging purposes and can be safely ignored. Finally, in the last few lines of block 3, the data are reduced and printed. The reduce command is what enables this fix to run massively in parallel as it gathers all the data computed on individual Message Passing Interface (MPI) processes (e.g., individual cores or nodes) and brings it to a single node that will perform the writing/printing operation to a file.

The compute *gkma* code has been written so that users can bin modal information about a system. That is, rather

than obtaining information about every individual mode's heat flux, the user can use compute *gkma* to obtain the heat flux due to one or several bins of modes. Binning is important for large systems, which require large amounts of memory to store modal heat fluxes and long job wall-times to continually write modal heat flux information. Thus far, the binning process is limited to modes that are adjacent in the *eigvector.eig* file. Thus, unless the eigenvector file is modified, binning will always occur for modes with sequential frequencies.

To perform a compute *gkma* calculation, the user should follow all procedures for running a compute *heat/flux* calculation, i.e., initialize *ke/atom*, *pe/atom*, and *stress/atom* computes and use them as arguments for the compute *gkma* command. As mentioned previously, the user should also ensure a file named "eigvector.eig" is located in the same directory as other LAMMPS input files. The command compute *gkma* in the LAMMPS input is formatted identically to that of compute *heat/flux*, except that the user should also supply information about binning at the end of the command. This information should be formatted as three integers, identified in the compute *gkma* code as *firstmode*, *lastmode*, and *binsize*. These quantities are self-explanatory: *firstmode* gives the first mode (based on the order of the modes in *eigvector.eig*) for which the user wishes to perform calculations, while *lastmode* gives the last mode for which the user is performing calculations; *binsize* is simply the number of modes to include in a single bin.

Assuming a 1000-atom system (and thus, 3000 total vibrational modes), some examples of how this command might be implemented are

```
compute modalflux all gkma myKE myPE myStress 1 3000 1
```

This command will provide information about every single mode in the system. It will not actually perform any binning, as the bin size is 1.

```
compute modalflux all gkma myKE myPE myStress 1 3000 3000
```

This command's output will be identical to "compute flux all *heat/flux* myKE myPE myStress." It computes modal heat fluxes for all modes but bins' contributions into a bin of 3000 modes (i.e., every mode in the system). This single output is therefore the sum of all modal contributions and will exactly recover the bulk (i.e., not modal) heat fluxes.

```
compute modalflux all gkma myKE myPE myStress 1 1000 100
```

Assuming no modification of the *eigvector.eig* file, this command will compute the modal heat fluxes of the first 1000 modes with the lowest frequencies (as modes are sorted by frequency in the *eigvector.eig* file output by GULP). There will be 10 heat fluxes output at each timestep. The first value is the sum of contributions from the 100 lowest frequency modes, etc.

The user should take care that the bin size exactly divides the total number of bins being examined, i.e.,  $\text{mod}(\text{lastbin} - \text{firstbin} + 1, \text{binsize}) = 0$ . While the code will still run if this

condition is not met, we have not examined the output in such a case, and we expect the heat flux values for at least one bin will be incorrect.

For the computes listed above (i.e., a *gkma* compute named "modalflux"), the values from the *gkma* compute can be output via the command

```
fix my_ave1 all ave/time Nevery Nrepeat Nfreq c_modalflux[*]  
file modal_output.txt mode vector
```

where the output file is named "modal\_output.txt." (The user can pick any name for both the compute itself and the output file.) The quantities *Nevery* *Nrepeat* *Nfreq* are explained in the LAMMPS documentation of *fix ave/time*.

Many high-performance computing infrastructures use job schedulers to prioritize and schedule jobs. Many schedulers are configured to give priority to smaller jobs that request less processors and a smaller wall time. For this reason, on such infrastructures, it can be useful to break a single MD-GKMA trajectory into many separate yet identical evaluations of the same trajectory where each is responsible for tracking and recording a subset of the modes level heat fluxes. Overall, this results in a greater computational expense, but in practice it can yield the results in less time, since the GKMA portion of the code can be many times more expensive than the base MD portion. When in this regime, it can be computationally expensive, due to the large number of simulations required to obtain the TC accumulation function. For instance, for a system with *N* atoms, rather than calculating all  $3N$  modal information from a single simulation, up to  $3N$  parallel simulations corresponding to the total number of vibrational modes in the system can be run to obtain the TC accumulation function. It can also be expensive because of the large MD simulation time needed (i.e., typically  $>5$  ns) for each of  $3N$  simulations to decrease the statistical error associated with correlation functions. This, however, can be reduced by reducing the frequency of the mode heat current calculations. For example, instead of calculating the heat flux every time step during the simulation, one can calculate the heat flux every 10 time steps, which can reduce the cost associated with the GKMA by  $10\times$ . The necessary output frequency can be estimated by first calculating the total TC using GK for various output frequencies, i.e., by simply recording the heat flux at every step for a MD run and then in postprocessing using a code that simply samples the recorded data at the desired frequency. In this was one can repeat the postprocessing calculations to quickly determine the lowest output frequency at which the TC remains converged to the same value associated with outputting at every step.

As discussed previously, one can also bin modes together to decrease the total number of simulations needed. Since in Eq. (9) the individual mode level detail is retained, one can sum any group of desired modes to obtain their net contribution at one time. This can significantly reduce the computational time and storage requirements for the calculation and it can enable more tractable scaling  $3NN_{\text{bin}}$  vs.  $3N^2$ , where  $N_{\text{bin}}$  is the desired resolution, e.g., 100 bins across the entire

frequency regime. For instance, one can sum the contribution of all acoustic modes in crystalline materials and calculate their TC contribution all at once via

$$\kappa_{\alpha\beta,n} = \frac{V}{k_b T^2} \int \left\langle \sum_n^{\text{acoustic}} \mathbf{Q}_{\alpha,n}(t+t') \mathbf{Q}_{\beta,n}(t) \right\rangle dt'. \quad (21)$$

Such a simplification is useful, because very often there may be a group of modes that are of primary interest, and individual mode level detail can be targeted on such groups, while other modes such as optical modes, which may have minimal contributions to the TC,<sup>45</sup> can be assessed as a single group or can be simply neglected. It is important to mention that mathematically the correlation between combined mode heat fluxes and the total heat flux is exactly equal to the sum of all of the correlations between individual heat fluxes and the total heat flux. The only difference this combination scheme will make is on the specific heat correction. For example, if the number of bins used in frequency is too small, and thus a single bin represents a group of modes with a wide frequency range, the quantum correction could be highly inaccurate because it may not be clear what single frequency should be used to represent the entire group. Therefore, another approach that can be used to reduce computational expense is to compute a group of modes of interest and obtain the contributions associated with all remaining modes at once, by simply subtracting the heat flux associated with the target group from the total. In this one step, one can obtain the time dependent heat flux of all modes that were not specifically computed in a given trajectory, by simply subtracting the computed modes from the total heat flux.

When applying the quantum correction, one can use the averaged frequency of the combined modes in one interval to calculate the specific heat suppression. In practice, for any given material, the user first needs to study how the system size and total simulation time affect the total TC calculated, using the less expensive GK method alone. Once the optimum system size and simulation time is obtained for converged results, the frequency spectrum of the system of interest can be divided into  $M$  bins (e.g., usually 100–200), in which a variable number of modes are included in each bin, based on the density of states. Then,  $M$  simulations are conducted in which the heat fluxes are written to a file every 10–20 time steps. Once all  $M$  simulations are finished, the correlation functions can be calculated which can later be plotted versus average mode frequency in each bin to obtain TC spectrum. Another more computationally balanced approach that has not yet been implemented would be to use the constant number of modes in each bin. This, however, would result in non-uniformity in frequency space or the dimension of a descriptor of interest. Nonetheless, this might provide a more computationally balanced approach, but in practice, since all of the parallel instances of the trajectory do not usually run at the same time, it is quite acceptable to just wait for all the instances to finish. This is because longer runs with more modes are likely to be followed by other simulations that started later, and

therefore they are not usually the last to finish. It is worth noting that when distributing the modal calculations amongst different jobs, the same random velocities (i.e., random seed values) must be used for all the simulations so that all the calculated modal contributions correspond to the same trajectory in the  $6N$ -dimension phase-space<sup>31,46</sup> (i.e.,  $3N$  dimensions for position and  $3N$  dimensions for momentum variables).

Finally, the computational time required to perform harmonic LD calculation depends on the number of atoms in the unit cell. The time required for the Gamma point calculations scales as  $N^3$  and the required memory scales as  $N^2$ , where  $N$  is the total number of atoms in the supercell. This scaling can impede the study of systems with a large number of atoms (>10 000), as is required for disordered materials such as amorphous solids and random alloys, for which the calculations will take >1 day given current high-performance computing hardware. However, the LD calculation is parallelizable and can be performed using the Portable, Extensible Toolkit for Scientific Computation (PETSc) or the Scalable Linear Algebra Package (SCALAPACK), which both have routines for performing eigenvalue solutions in parallel. For minimization purposes, when using efficiently parallel MD algorithms (e.g., the open-source LAMMPS package<sup>41</sup>), the simulation time scales linearly with  $N$ , while the memory scales with  $N^2$ . For example, for a system with  $10^5$  atoms, there are  $9 \times 10^{10}$  elements in the dynamical matrix. Assuming 8 bytes per element, the total memory required for the calculation is 720 GB. However, if the calculation is distributed over 200 cores, then each core only needs 3.6 GB, which is tractable for current hardware.

## E. Sample case studies using GKMA

In this section, we will present example results for the temperature dependent TC calculation of homogeneous crystalline solids, amorphous, and random alloys. The results demonstrate the ability of GKMA in predicting the TC of various systems.

### 1. Validation with a crystalline solid

Prior to explicit validation, it was hypothesized, but not proven that the mode level quantity in Eq. (10) actually corresponded to that mode's contribution to TC. For example, prior work postulated that the frequency content of the HFAC might be associated with phonons at the corresponding frequency.<sup>47,48</sup> However, it is now more widely appreciated that the frequency content of the HFAC, i.e., the components obtained from a Fourier Transform of the HFAC, instead correspond to the frequency of the thermal perturbation. Thus, it was not clear *a priori*, that if one were to compute mode level components, as is done in Eq. (10), that these quantities would in fact correspond to the mode level contributions to TC. To test this, Lv and Henry<sup>4</sup> compared the GKMA results for crystalline silicon (c-Si) using the Tersoff potential<sup>49</sup> with other well established methods.<sup>34,50,51</sup> In their simulation, they employed periodic boundary conditions in all directions. Each simulation began with equilibration under temperature control using velocity-rescaling [using ensembles held at

constant atom number, pressure, and temperature (NPT) and constant atom number, volume, and temperature (NVT)] for 100 ps. After an initial equilibration period, the modal heat fluxes and other modal information were computed at equilibrium in an ensemble held at constant atom number, volume, and energy (NVE, or the microcanonical ensemble) for 10 ns, without temperature control. Figure 1(a) shows the normalized TC accumulation for c-Si calculated using GKMA compared to the one computed using the normal mode analysis (NMA) method using the Tersoff empirical potential. As seen, the shapes of both the GKMA and NMA accumulations are similar and exhibit the same types of features. As shown in Fig. 1(b), GKMA prediction of the TC contributions for different branches is also close to the first principles and NMA results. It can be seen that PGM-based methods predict zero contribution of TO mode to the TC, while the GKMA approach ascribes a slightly negative value. Here, it should be mentioned that in the context of GKMA it is possible for a mode to exhibit a negative contribution to TC. Conceptually, this can occur when the fluctuations in a mode's heat flux are anti-correlated (i.e., out of phase), with the total heat flow. This can be true for individual modes, but in practice the total TC is always positive, as is required by the second law of thermodynamics. Lastly, as seen the GKMA accumulation results in Fig. 1, there is general agreement with first principles calculations using density functional theory (DFT)<sup>51</sup> and previous work using the environment dependent interatomic potential (EDIP).<sup>52</sup> Since both EDIP and Tersoff are short ranged empirical potentials, it seems reasonable that the agreement between them might be better than with DFT, which includes longer ranged interactions and is more accurate. Ideally, these calculations should be repeated with all three methods (i.e., NMA, 3-Phonon scattering rate via Fermi's Golden Rule,<sup>51</sup> and GKMA) evaluated using the exact

same potential, and this is a target for future work. In this way, any discrepancies between the three can be considered in more detail. Nonetheless, this initial validation of GKMA has offered significant evidence to suggest that the mode level components to TC obtained from Eq. (10) do in fact correspond to the phonon/individual mode contributions.

## 2. Amorphous solids

The GKMA method can also be applied to amorphous solids. For example, Lv and Henry<sup>4-7</sup> applied the GKMA to analyze the modal contributions to TC in amorphous silicon (a-Si), amorphous carbon (a-C), and amorphous silica (a-SiO<sub>2</sub>), where propagons, diffusons, and locons are all treated the same way. Here, it is important to note that Allen and Feldman (AF) in 1993 developed a harmonic method to calculate the contributions of diffusons to the TC<sup>53</sup> using the GK formula. In their work, they assumed a functional form for the interactions between atoms, which was harmonic in form, i.e., the forces on atoms linearly increased with their displacement away from equilibrium. Nonetheless, by making this assumption they were able to evaluate the HFAC in closed form, thereby resulting in a closed form expression for the mode level TC contributions. From this perspective, it becomes clear that GKMA essentially follows the same procedure as the AF by decomposing the heat current into its mode level contributions, although GKMA was conceived of and developed independently. The main difference is that GKMA makes no intrinsic assumption about the form of the potential, and therefore it requires an explicit evaluation of the potential, e.g., via MD simulations. The benefit of this approach is that the resulting mode level TC contributions then naturally include anharmonicity to full order. With this in mind, one can then assess the contribution of anharmonicity to the TC by comparing AF and GKMA results. For amorphous

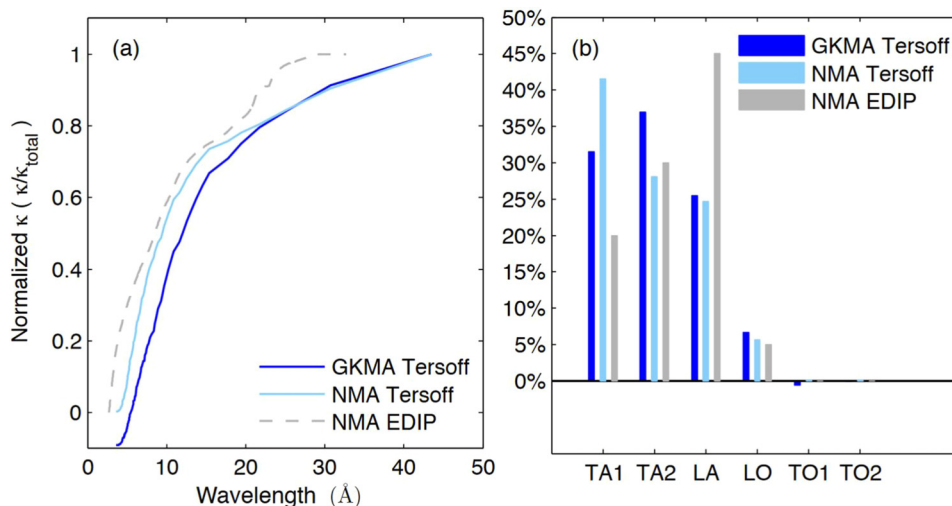


**FIG. 1.** (a) TC of c-Si accumulation with wavelength. (b) Comparison of each phonon polarization's contribution to the TC of c-Si. The six polarizations are the transverse acoustic (TA), longitudinal acoustic (LA), transverse optical (TO), and longitudinal optical (LO). The presented modal contributions in this figure are not quantum corrected.

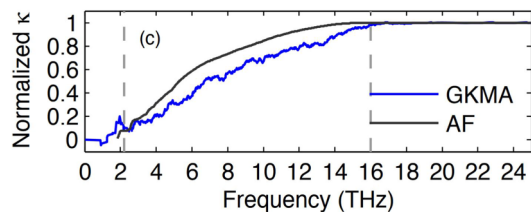


**FIG. 2.** Normalized TC accumulation vs. mode frequency for a-Si at 300 K using GKMA and AF theory at 300 K. The dotted gray lines are estimated transition between propagons and diffusons and between diffusons and locons, based on direct inspection of the mode character. The presented modal contributions in this figure are not quantum corrected.

silicon (a-Si), Lv and Henry<sup>4</sup> used this approach to assess how important anharmonicity is and they also calculated the TC accumulation function for all modes versus phonon frequency. As seen in Fig. 2, GKMA predicts a similar trend as the AF result at room temperature, which does not incorporate the effects of anharmonicity on the mode–mode interactions. At first, this might seem to suggest that anharmonicity is not important. However, examination of the 2D cross-correlation terms shown in Fig. 3 indicates that there is significant correlation between modes with different frequencies. In Fig. 3(a), the diagonal terms are the largest, but they only account for ~70% of the total TC at room temperature.

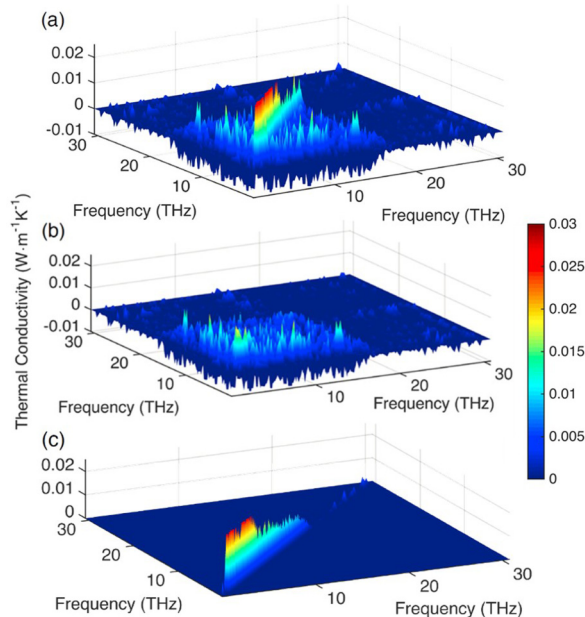


**FIG. 3.** (a) TC contributions from mode-mode correlations of amorphous silicon; (b) TC contributions from just mode-mode cross-correlations of amorphous silicon; (c) TC contributions from only mode-mode auto-correlations of amorphous silicon. The presented modal contributions in this figure are not quantum corrected.

Figure 4 shows the effect of applying quantum corrections to classical MD results via Eq. (16) for an amorphous silica system.<sup>6</sup> The data in Fig. 4(a) correspond to evaluating Eq. (16) and setting, i.e.,  $f_Q = 1$ , whereas Fig. 4(b) shows the same data for values of  $f_Q$  equal to the quantum vs. classical specific heat ratio. Frequencies are taken from the values of  $\omega_0$  obtained from a 0 K LD calculation; similarly, values of  $f_k$  are assumed not to be temperature dependent and are simply the values calculated for a system at 400 K. In reality, modes will experience frequency softening, which leads to a slight reduction in mode frequency at high temperatures. The effect of this softening is shown in Fig. 4(c). Furthermore,  $f_k$  is a function of temperature, and values should be calculated at different temperatures; Fig. 4(d) shows the improvement in TC at different temperatures achieved by calculating  $f_k$  at the relevant temperature. Further discussion of these points may be found in the original paper by Lv and Henry.<sup>6</sup>

### 3. Random alloys

The current theory for phonon transport in alloys is based on the VCA,<sup>10</sup> which is based on PGM. However, Seyf et al.<sup>19</sup> in their recent study showed that the normal modes in

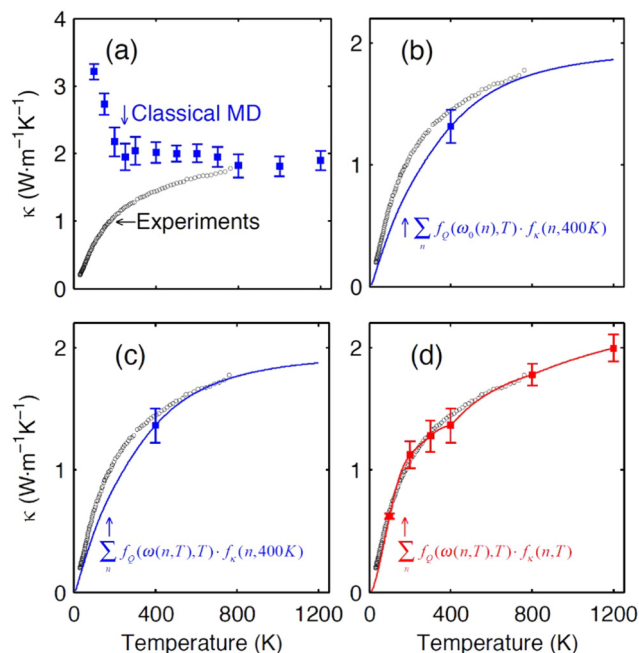


**FIG. 4.** Panel (a) shows the GK results with error bars comparing with experiments (black circles). The error bars correspond to the standard deviations observed for independent ensembles; (b) is the result of using 400 K GKMA data with quantum specific heat correction; (c) is based on the results in (b) with the addition of temperature dependent frequencies at 400 K; (d) shows the TC using GKMA results at 100 K, 200 K, 300 K, 400 K, 800 K, and 1200 K (interpolated in between) with the quantum specific heat correction and temperature dependent frequencies. Taken from Ref. 6.

a crystalline random InGaAs alloy fall into the same three categories identified by Allen and Feldman in 1999 for amorphous materials, namely, propagons, diffusons, and locons.<sup>54</sup> They showed all modes do not propagate and hence one would expect PGM-based theories/models may breakdown for alloys with larger degree of compositional impurities, i.e., 15%–85% composition range. To calculate the contribution of different categories of vibrational modes in the system, they used GKMA. Figure 5 shows the temperature dependent TC of  $\text{In}_{0.53}\text{Ga}_{0.47}\text{As}$  film<sup>19</sup> and the corresponding theoretical predictions using GKMA. Each labeled curve highlights the respective contributions associated with propagons, diffusons, and locons. In their study, the localized modes were identified using the participation ratio,<sup>55</sup> while the propagating modes were identified using “Eigenvector Periodicity Analysis (EPA).”<sup>56</sup> Essentially, EPA measures the degree of periodicity of a given vibrational modes compared to a pure 100% propagating phonon and a universal transition value of 20% periodicity was suggested as a distinction between propagons and non-propagons. After identifying propagons, diffusons, and locons in the system, the TC corresponding for each category of modes is calculated as shown in Fig. 5.

In the first half of this tutorial, we have introduced a correlation based modal analysis method, i.e., GKMA to understand and calculate the TC from atomistic level simulations. Importantly, the results using GKMA have produced good agreement with experiments for several amorphous materials and a random alloy, as shown in Fig. 6. What is noteworthy about the data in Fig. 6 is the fact that all of the phonon contributions in all of the materials were computed with the

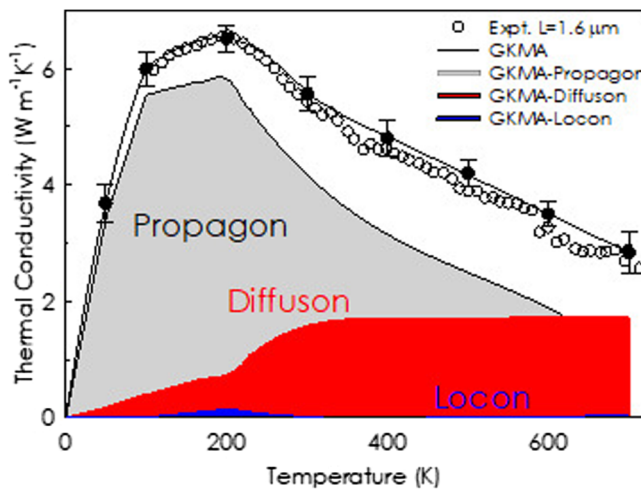


**FIG. 5.** TC of  $\text{In}_{0.53}\text{Ga}_{0.47}\text{As}$ . Temperature dependent TC of  $\text{In}_{0.53}\text{Ga}_{0.47}\text{As}$  film<sup>19</sup> and the corresponding theoretical predictions using GKMA. The error bars were determined based on the standard deviation of GK results at a given temperature. Each labeled curve highlights the respective contributions associated with propagons, diffusons, and locons, according to the GKMA and EPA methodologies.<sup>19,56</sup>

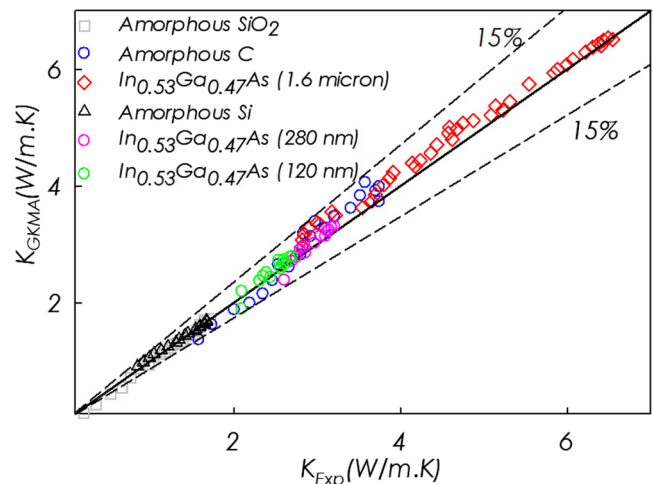


**FIG. 6.** GKMA TC predictions for various solids.

exact same formalism, without any modification. This means that GKMA provides a unified formalism with which phonons can be understood in any material system where atoms vibrate around equilibrium positions, including individual molecules.<sup>57</sup> GKMA still has yet to be applied and validated for some systems, particularly highly disordered systems including amorphous polymers and materials with a high concentration of defects, though work is underway to study such systems within the GKMA framework.

### III. INTERFACE CONDUCTANCE MODAL ANALYSIS

In this section, we present the ICMA formalism, which is an approach for TIC calculation based on MD.<sup>3,23</sup> Based on MD, ICMA (i) fully includes anharmonicity through sampling of a naturally anharmonic interatomic potential, (ii) can be applied to different detailed atomic configurations around interface (i.e., including defects or varying degrees of lattice mismatch), and (iii) does not make use of any definition of group velocity, since it does not making any assumptions about the physical picture for phonons. As will be shown in Secs. III A–III D, ICMA is based on correlation description of phonon interactions and can be applied to interfaces involving any combination of rigid bodies.

#### A. ICMA formulation in EMD

Consider forming an interface by bringing into contact two solids A and B, each having  $N_A$  and  $N_B$  atoms, respectively. We can use LD calculations<sup>37</sup> to obtain the complete  $3N = 3(N_A + N_B)$  eigen solutions to the equations of motion describing the vibrations of the combined system of two materials. To find the contributions of these eigen modes to the TIC, we first need to determine their contributions to the interfacial heat flow. Interfacial heat flow between two solids is the net

energy exchanged between the atoms on the opposite sides of the interface, which can be found by examining the rate of energy (i.e., Hamiltonian) change for individual atoms in the system. The total Hamiltonian ( $H$ ) for a system of  $N = N_A + N_B$  atoms is given by<sup>36</sup>

$$H = \sum_i^N \frac{\mathbf{p}_i^2}{2m_i} + \Phi(\mathbf{r}_1, \mathbf{r}_2, \dots, \mathbf{r}_n), \quad (22)$$

where  $\Phi$  is the total potential energy of the system, and  $\mathbf{r}_i$  and  $\mathbf{p}_i$  are the position and momentum of atom  $i$ , respectively. From Eq. (22), the individual Hamiltonian for atom  $i$  can be written as

$$H_i = \frac{\mathbf{p}_i^2}{2m_i} + \Phi_i(\mathbf{r}_1, \mathbf{r}_2, \dots, \mathbf{r}_n), \quad (23)$$

where  $\Phi_i$  is the potential energy assigned to the individual atom  $i$  with the condition that  $\sum_i^N \Phi_i = \Phi$ .<sup>34,36</sup> The time-derivative of Eq. (23) yields the rate of change in the energy of atom  $i$ ,

$$\begin{aligned} \frac{\partial H_i}{\partial t} &= \frac{\partial H_i}{\partial \mathbf{p}_i} \cdot \left( \frac{d\mathbf{p}_i}{dt} \right) + \sum_n^N \frac{\partial H_i}{\partial \mathbf{r}_n} \cdot \frac{d\mathbf{r}_n}{dt} \\ &= \frac{\mathbf{p}_i}{m_i} \cdot \left( \frac{d\mathbf{p}_i}{dt} \right) + \sum_n^N \frac{\partial \Phi_i}{\partial \mathbf{r}_n} \cdot \frac{d\mathbf{r}_n}{dt}. \end{aligned} \quad (24)$$

Following Fig. 7, if we consider that atom  $i$  is on side A, it has interactions with atoms on the same side (e.g., atom  $k$  in Fig. 7)

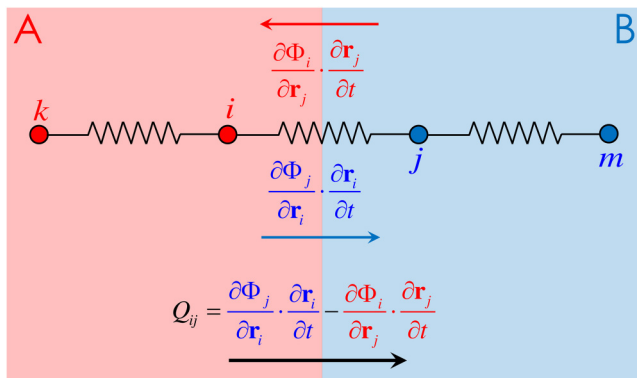


**FIG. 7.** A representative interface formed by joining two solids A and B.  $Q_{ij}$  is the net amount of exchanged heat between atom  $i$  on side A and atom  $j$  on side B. Total interfacial heat flow will then be  $Q = \sum_{i \in A} \sum_{j \in B} Q_{ij}$ . The definition for

$Q$  has two terms. The first term (blue) originates from the definition for the rate of energy change for atom  $j$  and when positive, it represents heat conduction from side A to side B, schematically shown by the blue arrow. The second term (red) originates from the definition for the rate of energy change for atom  $i$  and when positive, it represents heat conduction from side B to side A, schematically shown by the red arrow.

and atoms on the other side (e.g., atom  $j$  in Fig. 7). This leads us to expand Eq. (24) in the following form:

$$\frac{\partial H_i}{\partial t} = \frac{\mathbf{p}_i}{m_i} \cdot \left( \frac{d\mathbf{p}_i}{dt} \right) + \frac{\partial \Phi_i}{\partial \mathbf{r}_i} \cdot \frac{d\mathbf{r}_i}{dt} + \sum_{k \in A, k \neq i}^{N_A} \frac{\partial \Phi_i}{\partial \mathbf{r}_k} \cdot \frac{d\mathbf{r}_k}{dt} + \sum_{j \in B}^{N_B} \frac{\partial \Phi_i}{\partial \mathbf{r}_j} \cdot \frac{d\mathbf{r}_j}{dt}. \quad (25)$$

The first and second terms in Eq. (25) correspond to the change in the kinetic energy of atom  $i$  and its self-interaction.<sup>37</sup> The third and fourth terms represent the interactions of atom  $i$  with atoms on the same side (A) and with atoms on the opposite side (B). Among these terms, only the fourth term (i.e., interactions with atoms on the other side of the interface) contributes to the interfacial heat flow. Rewriting Eq. (25) for atom  $j$  on side B results in the following formula:

$$\begin{aligned} \frac{\partial H_j}{\partial t} &= \frac{\mathbf{p}_j}{m_j} \cdot \left( \frac{d\mathbf{p}_j}{dt} \right) + \frac{\partial \Phi_j}{\partial \mathbf{r}_j} \cdot \frac{d\mathbf{r}_j}{dt} + \sum_{m \in B, m \neq j}^{N_B} \frac{\partial \Phi_j}{\partial \mathbf{r}_m} \cdot \frac{d\mathbf{r}_m}{dt} \\ &\quad + \sum_{i \in A}^{N_A} \frac{\partial \Phi_j}{\partial \mathbf{r}_i} \cdot \frac{d\mathbf{r}_i}{dt}, \end{aligned} \quad (26)$$

where again the fourth term is the only one that contributes to the interfacial heat flow.

As is schematically shown in Fig. 7, if individual components in the fourth terms of Eqs. (25) and (26) are positive, they transfer energy from side B to side A and from side A to B, respectively. Thus, if we take the positive sign for total interfacial heat flow to be the heat conduction from side A to B, the fourth terms in Eqs. (25) and (26) can be added together with the opposite signs to result in the following definition for the instantaneous heat flow between materials A and B ( $Q$ ),<sup>58-60</sup>

$$Q = \sum_{i \in A}^{N_A} \sum_{j \in B}^{N_B} \left\{ \frac{\partial \Phi_j}{\partial \mathbf{r}_i} \cdot \frac{d\mathbf{r}_i}{dt} - \frac{\partial \Phi_i}{\partial \mathbf{r}_j} \cdot \frac{d\mathbf{r}_j}{dt} \right\}. \quad (27)$$

In the above formula,  $\frac{d\mathbf{r}_i}{dt}$  is the velocity of atom  $i$  (i.e.,  $\dot{\mathbf{x}}_i$ ), and  $-\frac{\partial \Phi_i}{\partial \mathbf{r}_i}$  is proportional to the force exerted on atom  $i$  by interaction with atom  $j$  (i.e.,  $\mathbf{f}_{ij}$ ) and vice versa. For the common case of having pairwise interactions between materials A and B where the interaction energy ( $\Phi_{ij}$ ) is equally distributed between atoms  $i$  and  $j$ , we have the following relations between the forces and potential energies:

$$-\frac{\partial \Phi_j}{\partial \mathbf{r}_i} = -\frac{1}{2} \frac{\partial \Phi_{ij}}{\partial \mathbf{r}_i} = \frac{1}{2} \mathbf{f}_{ij} = -\frac{1}{2} \mathbf{f}_{ji} = \frac{1}{2} \frac{\partial \Phi_{ij}}{\partial \mathbf{r}_j} = \frac{\partial \Phi_i}{\partial \mathbf{r}_j}. \quad (28)$$

Using the above relations, Eq. (27) reduces to<sup>59,61,62</sup>

$$Q = -\frac{1}{2} \sum_{i \in A}^{N_A} \sum_{j \in B}^{N_B} \mathbf{f}_{ij} \cdot (\dot{\mathbf{x}}_i + \dot{\mathbf{x}}_j). \quad (29)$$

To determine the modal contributions to heat flow ( $Q_n$ ), with the requirement of  $Q = \sum_n Q_n$ , using the same process as GKMA, we replace the atomic velocities in Eq. (27) with their modal definition from Eq. (7),

$$Q = \sum_{i \in A} \sum_{j \in B} \left[ \left( \frac{\partial \Phi_j}{\partial r_i} \right) \cdot \left( \sum_n \frac{1}{(m_i)^{1/2}} \mathbf{e}_{n,i} \dot{X}_n \right) - \left( \frac{\partial \Phi_i}{\partial r_j} \right) \cdot \left( \sum_n \frac{1}{(m_j)^{1/2}} \mathbf{e}_{n,j} \dot{X}_n \right) \right], \quad (30)$$

$$Q_n = \sum_{i \in A} \sum_{j \in B} \left[ \left( \frac{\partial \Phi_j}{\partial r_i} \right) \cdot \left( \frac{1}{(m_i)^{1/2}} \mathbf{e}_{n,i} \dot{X}_n \right) + \left( \frac{-\partial \Phi_i}{\partial r_j} \right) \cdot \left( \frac{1}{(m_j)^{1/2}} \mathbf{e}_{n,j} \dot{X}_n \right) \right]. \quad (31)$$

Equation (31) is general, and it can be simplified to the following form for the pairwise interactions:

$$Q_n = \sum_{i \in A} \sum_{j \in B} \frac{-\mathbf{f}_{ij}}{2} \cdot \left( \frac{1}{(m_i)^{1/2}} \mathbf{e}_{n,i} \dot{X}_n + \frac{1}{(m_j)^{1/2}} \mathbf{e}_{n,j} \dot{X}_n \right). \quad (32)$$

Equations (31) and (32) are the modal contributions to the interfacial heat flow and can be replaced in any definition of TIC to obtain the modal contributions to TIC ( $G_n$ ), where  $G = \sum G_n$ . In EMD simulations, calculation of TIC follows the fluctuation-dissipation theorem.<sup>63</sup> In this approach, TIC is proportional to the auto-correlation of the equilibrium fluctuations of heat flux across the interface based on the following formula:

$$G = \frac{1}{Ak_B T^2} \int_0^\infty \langle Q(t)Q(0) \rangle dt, \quad (33)$$

where  $A$  is the interface contact area,  $k_B$  is the Boltzmann constant,  $T$  is the equilibrium temperature of the system,  $Q$  is the instantaneous interfacial heat flow, and  $\langle \dots \rangle$  represents the autocorrelation function. By replacing the modal contributions to heat flow in one of the heat flows in Eq. (33), we have

$$G = \frac{1}{Ak_B T^2} \int \left\langle \sum_n Q_n(t)Q(0) \right\rangle dt \\ = \sum_n \frac{1}{Ak_B T^2} \int \langle Q_n(t)Q(0) \rangle dt, \quad (34)$$

$$G_n = \frac{1}{Ak_B T^2} \int \langle Q_n(t)Q(0) \rangle dt. \quad (35)$$

If one sorts the vibrational modes ( $n$ ) based on their frequencies, the modal contributions to TIC in Eq. (35) can then be shown in the form of a frequency-based TIC accumulation function (see Fig. 11 as representative examples). Furthermore, by substituting for both heat flows in Eq. (33), another definition for modal contributions to  $G$  can be

obtained as

$$G = \frac{1}{Ak_B T^2} \int \left\langle \sum_n Q_n(t) \sum_{n'} Q_{n'}(t) \right\rangle dt \\ = \sum_n \sum_{n'} \frac{1}{Ak_B T^2} \int \langle Q_n(t)Q_{n'}(0) \rangle dt, \quad (36)$$

where individual contributions to TIC from pairs of modes ( $G_{n,n'}$ ) are found to be

$$G_{n,n'} = \frac{1}{Ak_B T^2} \int \langle Q_n(t)Q_{n'}(0) \rangle dt. \quad (37)$$

The pairwise modal contributions obtained by Eq. (37) are often reflected on 2D correlation maps, where the two axes of the map follow the frequencies of modes  $n$  and  $n'$  (see Fig. 13 as representative examples). Equations (35) and (37) are the modal contributions to the TIC from its equilibrium definition in EMD simulations.

Before using Eqs. (35) and (37) to study the heat conduction across different interfaces in Subsections III D 1 and III D 2, we discuss the following four issues, which are critical for the correct implementation of ICMA formalism and better understanding of its underlying foundation. First, we examine different choices of basis set and discuss the correct one that should be used with Eqs. (31) and (32). Second, we show that the modes of vibration belonging to the correct basis set do not resemble the conventional picture of phonons as sinusoidally propagating waves. In this regard, to facilitate a more structured analysis of these vibrational modes around interfaces, we classify them into different categories. Third, we note that the modal contribution formulas in Eqs. (31) and (32) were obtained by modal decomposition of atomic velocities. In Subsection III A 3, we examine if other definitions of modal contributions to TIC can be found by modal analysis of atomic forces. Lastly, we discuss the different viewpoint coming from the correlation-based foundation of the modal decompositions presented in Eqs. (35) and (37).

### 1. The correct choice of basis set

The modal contributions to interfacial heat flow from Eq. (31) are based on atomic velocities and eigen modes of

vibration from both sides of the interface. Such a description for interfacial heat flow is inconsistent with the conventional treatment of interfacial heat transfer, whereby all the parameters required to describe the interfacial transport are obtained from the vibrational information belonging to only one side of the interface.<sup>1,58</sup> One can potentially resolve this inconsistency by instead using the following equations for total and modal instantaneous interfacial heat flow values:

$$Q = \sum_{i \in A} \sum_{j \in B} \frac{\partial \Phi_j}{\partial \mathbf{r}_i} \cdot \frac{d\mathbf{r}_i}{dt}, \quad (38)$$

$$Q_n = \frac{1}{N^{1/2}} \sum_{i \in A} \sum_{j \in B} \left( \frac{\partial \Phi_j}{\partial \mathbf{r}_i} \right) \cdot \left( \frac{1}{(m_i)^{1/2}} \mathbf{e}_{n,i} \dot{X}_n \right). \quad (39)$$

The above equations are only based on atomic velocities and eigen modes of vibration from one side of the interface and are obtained from Eq. (27) by ascribing the interaction potential energy only to the atoms on one side of the interface (e.g.,  $\Phi_j = \Phi_{ij}$  and  $\Phi_i = 0$ ). Modal contributions to interfacial heat flow can be calculated using either Eqs. (31) or (38), but each of these equations requires a different basis set (i.e., set of eigen modes of vibration) as Eq. (31) is based on vibrational information from both sides of the interface and Eq. (38) is based on vibrational information from only one side of the interface. The key question then becomes, which basis set should one use in the heat flow decomposition to calculate physically meaningful contributions? This is important, since mathematically an arbitrary basis set can be complete, meaning that it returns the same total values of heat flow ( $Q = \sum_n Q_n$ ) and TIC ( $G = \sum_n G_n$ ), if it satisfies the following orthogonality relation:

$$\sum_i 2e_{n,i} \cdot 2e_{n',i} = \begin{cases} 0 & \text{if } n \neq n', \\ 1 & \text{if } n = n', \end{cases} \quad (40)$$

where index  $i$  denotes the atoms and indices  $n$  and  $n'$  represent the modes of vibration in the system. The condition above can theoretically be satisfied by an infinite number of arbitrary basis sets. The problem is that each of these mathematically complete basis sets can result in different descriptions for the contributions to heat flow and eventually TIC. This is critical, since by using a similar quantum correction scheme like the one described in Sec. III C, different spectral contributions to TIC then lead to different temperature dependent TIC predictions. Thus, the choice of basis set and specifically the assignment of different modes to certain frequencies is critical to properly interpreting the results.

As was argued in our prior reports on ICMA,<sup>3</sup> amongst the mathematically correct and infinite choices of basis set, the following three candidate basis sets were identified to have the greatest potential to also be physically correct. The first basis set includes the vibrational modes belonging to the bulk of either sides of the interface, where one calculates LD

only for one of the individual sides as a bulk material. The modes obtained from this basis set are used in Eq. (38). The second basis set also includes the vibrational modes for the bulk of individual sides of the interface; however, it combines these modes of vibration together, whereby it simply assigns polarization vectors equal to zero for the atoms on side B, when modes on side A are considered, and vice versa. Following this procedure, the second basis set candidate can be applied to Eq. (31). Finally, the third basis set corresponds to the modes obtained from a LD calculation on the entire structure, containing both materials A and B along with their interface.

To determine the correct basis set, Gordiz and Henry conducted a series of wave-packet (WP) simulations<sup>3</sup> whereby only a narrow range of frequencies with a single polarization is excited, and all other modes have zero amplitude which approximates  $T \rightarrow 0\text{K}$ . In this limit, the atomic interactions approach that of a perfectly harmonic potential, which means that modes can only transfer their energy to other modes with the same frequency. Thus, when the WP is launched toward the interface<sup>64,65</sup> and when it reaches the interface it elastically scatters. This condition translates into the requirement that the energy of the WP, before, during, and after the interaction by the interface is carried only by the modes of vibration with the same frequency as the ones in the initially excited narrow range of frequencies. Thus, all the non-zero reported modal contributions by a correct basis set should belong to the modes inside that narrow range of frequencies and all the other modes outside that range should have zero modal contributions. The first two basis sets that use vibrational information belonging only to one side of the interface fail to satisfy this requirement, where they report non-zero contributions to heat conduction by modes of vibration that were not included in the narrow range of frequencies. This is unphysical since these modes were not initially present and did not get excited during the simulation, as was confirmed by a simple FFT of the atom velocities. The only basis set that reported non-zero modal contributions only for the initially excited modes of vibration is the third basis set, for which the LD calculations were performed for the entirety of the structure including the interface and all its interactions. Thus, it became clear that this is the only correct basis set that should be used for all the modal decompositions based on ICMA formalism.

## 2. Classification of vibrational modes

Performing LD on the entire structure results in eigen modes of vibration that describe the natural collective motions for the whole interface system. Because of the broken symmetry in the system caused by interface, these collective motions can have eigen vectors of vibration that are different from the conventional picture of sinusoidally propagating phonons (see Fig. 8). To better study these modes of vibration, they can be classified into four main categories, based on the degree of localization of their vibrational energy

near the interface.<sup>3</sup> For instance, if more than 50% of the energy is around the interfacial region, the mode is classified interfacial, or if more than 90% of the energy is localized on one side of the interface and no vibrational energy is present around the interface region, the mode is classified as isolated. A framework for classifying these modes has been given elsewhere by Gordiz and Henry.<sup>3,58</sup>

### 3. Force decomposition approach

The obtained modal contributions to heat flow [Eq. (31)] and TIC [Eqs. (34) and (36)] are based on the modal decomposition of velocities. However, another approach can also be envisioned based on the modal decomposition of forces. The formulas for modal analysis based on force decomposition have been derived and reported in our previous study.<sup>58</sup> Like velocity decomposition, modal analysis based on force decomposition is also mathematically complete, however, one also needs to check whether the force decomposition approach physically meaningful. To check this, we conducted a similar WP test to the one that was discussed in Sec. III A

for determining the correct vibrational basis set. As the WP reaches the interface and starts interacting with it, non-zero contributions to heat flow arise in the force decomposition approach for modes of vibration with frequencies that lie outside the initially excited narrow range of frequencies. Since the interactions in the WP simulation are elastic and these non-zero contributions belong to the modes that are not even excited in the system, and since by construction, the only mode that can contribute is the one that is excited, this shows that the force decomposition does not correctly calculate the modal contributions to heat flow. Therefore, the velocity decomposition formulas seem to be the only ones that are both mathematically and physically correct and should be used for calculating the modal contributions to heat flow and TIC.

### 4. Correlation picture for interfacial heat transfer

The equilibrium definition of TIC [Eq. (33)] was first introduced by Puech *et al.*<sup>60</sup> and is in concept similar to the Green-Kubo technique for the calculation of TC from EMD

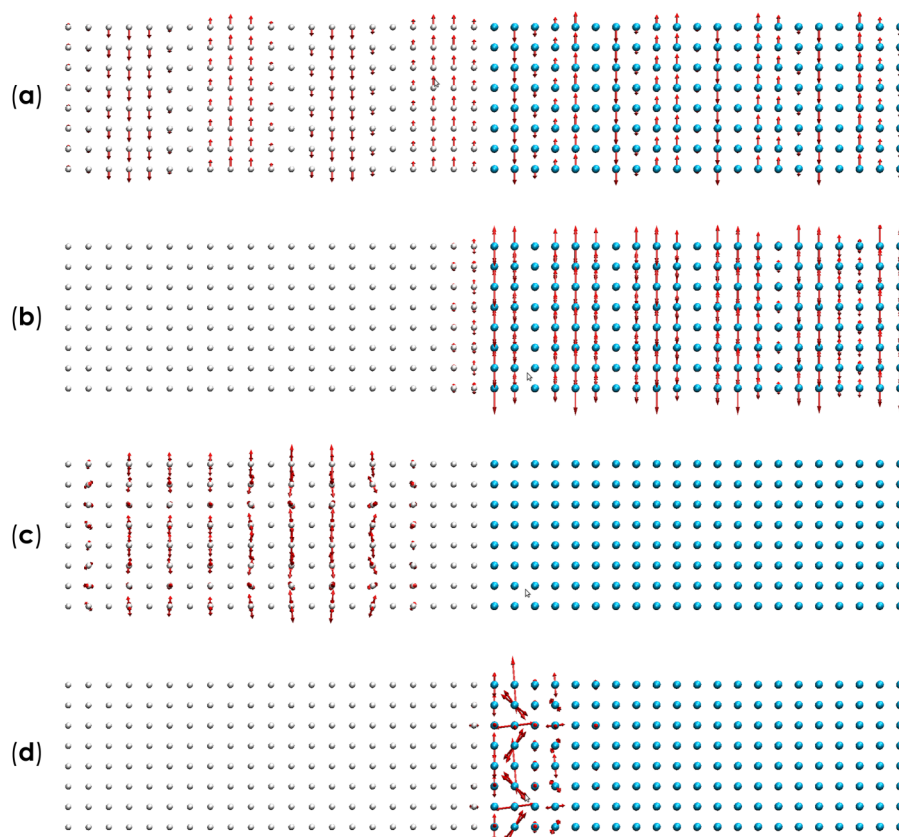


**FIG. 8.** Different classes of vibration across a solid-solid interface: (a) extended, (b) partially extended, (c) isolated, and (d) interfacial modes of vibration. The red arrows show the eigen vectors of vibration belonging to each atom in the structure. The presented interface is between lattice-matched mass-mismatched solid argon structures [Ar(m)/Ar(4m)]. White and cyan colors represent the argon and the heavy argon atoms, respectively.

simulations [Eq. (1)]. According to Eq. (33), TIC is directly proportional to the auto-correlation of the interfacial heat flow. If interfacial heat flow shows stronger correlation for a longer time, it will result in larger TIC. The ICMA formalism breaks down the auto-correlation of the interfacial heat flow in Eq. (33) to its underlying cross-correlations in Eqs. (35) and (37). What is particularly interesting is the definition in Eq. (37), where it represents TIC as the summation of all the cross-correlations between eigen mode pairs  $n$  and  $n'$  in the system ( $G = \sum G_{n,n'}$ ). Many modes of vibration can exist in the structure<sup>68,70</sup> and each pair can transfer the heat across the interface and contribute to TIC, if correlated. This correlation picture and its corresponding mathematical formulations [Eqs. (35) and (37)] have two important implications that may not necessarily agree with more well-established paradigms.

In the PGM picture, each mode of vibration can have a maximum contribution to TIC, when the entire energy of an incident phonon is transmitted to the other side of the interface and the transmission probability is unity (i.e.,  $\tau = 1$ ). However, according to the correlation picture in Eq. (37), no upper limit exists on the degree to which two modes of vibration can be correlated and contribute to TIC. In fact, for TC calculated from the GK method, it is possible to find structures, such as individual polymer chains, where some mode exhibit very long/strong correlations that can even lead to divergent TC.<sup>32</sup> Divergence has not been observed for TIC, but it is nonetheless important to note that mathematically it has no intrinsic upper bound.

The mathematical formulation provided in Eq. (37) even allows for negative contributions to TIC, because the fluctuations in the contribution to heat flux by two modes of vibration can become anti-correlated, which can lead to a negative contribution to TIC. Nonetheless, similar to GK/GKMA, the total TIC is in practice always positive, otherwise it would violate the second law. The above formulations complete the mathematical foundation of the ICMA method. Before discussing the computational cost considerations for ICMA in Sec. III C, Subsection III B discusses the non-equilibrium molecular dynamics (NEMD) implementation of ICMA.

## B. ICMA formulation in NEMD

For calculating TIC in NEMD simulations, a heat flow is forced to flow in the system and through the interface by placing hot and cold reservoirs in different locations in the system. As Fig. 9 shows, at steady state, a temperature profile forms in the structure and by directly measuring the temperature difference ( $\Delta T$ ) across the interface, TIC can be calculated using the  $G = \frac{\bar{Q}}{A \cdot \Delta T}$  formula, where  $\bar{Q}$  is the steady state, time-averaged interfacial heat flow in the NEMD simulation,  $A$  is the interface contact area, and  $\Delta T$  is the temperature difference at the interface, determined by extrapolation of the temperature gradients in each respective material<sup>66–69</sup> (see Fig. 9).

The modal contributions to the above NEMD definition of TIC ( $G_n$ ) can be readily obtained if the heat flow ( $Q$ ) is

replaced by its modal contributions ( $Q_n$ ),

$$G_n = \frac{\bar{Q}_n}{A \cdot \Delta T}, \quad (41)$$

where  $\Delta T$  is the same for all the vibrational modes. The above derivation is possible, since the definitions obtained for total [Eq. (27)] and modal [Eq. (32)] heat flow values are independent of the nature of the MD simulation; therefore, they can be used for both EMD and NEMD simulations. It should be noted that the obtained values of TIC from EMD are usually different from the ones from NEMD. However, the two values usually converge when the system size in NEMD is increased.<sup>29,71</sup> A similar difference between EMD and NEMD values has also been reported in TC calculations. For TC, these discrepancies are usually attributed to the scattering effect of heat baths in NEMD simulations, where it shortens the mean free path of phonons. However, for TIC, explaining the difference between EMD and NEMD values using the conventional PGM paradigm is challenging, since no direct length dependent property, such as phonon mean free path, enters the Landauer description for interfacial heat conduction.<sup>1</sup> The only indirect length-dependent property in the Landauer formula is the number of modes in the system, which increases by considering larger system sizes. This can potentially explain why increasing the size of the system in NEMD simulations help converge the TIC to its EMD counterpart, where the increased number of modes can reduce the effect of heat baths in the system until convergence is achieved, but convergence with respect to wavelength/mode extent typically happens within a few tens of nanometers.

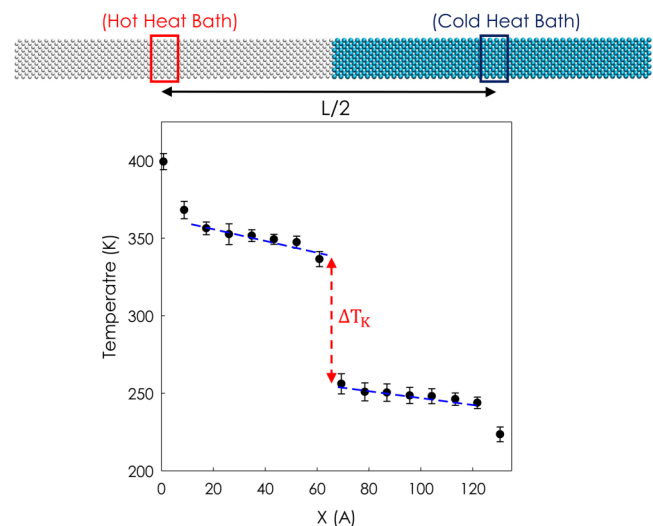


**FIG. 9.** Schematic of the NEMD implementation to calculate TIC across a representative c-Si (white atoms) and c-Ge (cyan atoms) interface structure.<sup>29</sup> Hot and cold heat baths are assigned by red and blue blocks, respectively. Temperature distribution is also provided, which clearly shows the temperature drop (Kapitza resistance<sup>70</sup>) across the interface.

In a study by Gordiz and Henry,<sup>29</sup> they investigated the heat conduction across all the possible interface combinations that can be obtained by joining dissimilar structures of crystalline (c-) and amorphous (a-) Si and Ge. The EMD results showed that the TIC for all these interfaces converged rather quickly with respect to the cross section and length of the system (typically around  $\sim 50$  nm). Based on previous reports,<sup>71</sup> the expectation was that the NEMD values would also converge to the EMD values, when the NEMD system size is increased. However, contrary to our expectation, NEMD TIC values for c-Si/c-Ge interface, unlike other interfaces, did not converge to their EMD counterparts and exhibited the strongest size dependence. In fact, perturbing the vibrations in this system by placing the heat baths at the bulk of the materials had a noticeable effect on TIC, even for a system with a total length of  $>120$  nm. Such an observation cannot be understood through the standard PGM/Landauer formalism, since it would be difficult to rationalize how perturbing a mode far from the interface would affect its transmissivity at the interface. However, as will be presented later in Sec. III D 2, ICMA calculations have shown that (i) the TIC at the c-Si/c-Ge interface is heavily dependent on a group of interfacial modes in the 12-13 THz frequency region<sup>27</sup> and (ii) a substantial portion of the vibration for these interfacial modes extends through the Si side (see Fig. 10). These two points explain that if one were to perform NEMD on c-Si/c-Ge interface, the heat baths artificially disrupt the natural vibrations and amplitudes of these highly contributing interfacial modes, which can hinder their ability to couple to other modes of vibration and transfer their energy to the other side of the interface, leading to a decreased TIC. Such an effect is interesting because it cannot be described by a scattering-based paradigm and could only be understood by the insight gained from ICMA calculations.

### C. Implementation and computational cost

In this section, we explain the implementation of ICMA through the modification of LAMMPS,<sup>41</sup> since it is the most widely used package for MD simulations. Many of the required steps and cost considerations for ICMA calculations are similar to that of GKMA, as explained in Sec. II D; when pertinent, the reader will be referred to Secs. III A and III B

for further explanation. The main goals in ICMA simulations are to calculate (i) the modal contributions to heat flow from Eqs. (31) and (32) and (ii) the individual and pairwise modal contributions to TIC from Eqs. (35) and (37). Similar to the GKMA approach, efficient calculations can be achieved if the modal heat fluxes are calculated and recorded first during the MD simulation and modal TIC values are determined by post-processing the recorded modal heat fluxes. All the necessary codes for conducting the ICMA calculation are provided in the [supplementary material](#). The provided codes and input files are extensively commented so they can be more easily understood and utilized in future implementations by the reader.

As was also discussed in the GKMA implementation section, two methods can be used to decrease the computational cost for modal analysis of a simulation of  $N$  atoms. First, one can divide the  $3N$  vibrational modes into separate groups and distribute them amongst computational nodes, where each computational node performs an identical simulation but outputs only the modal heat flow values for the modes assigned to it. Second, instead of calculating and recording the modal heat flow values at each time step in the simulation, one can calculate and record the modal contributions less frequently. In the current implementation of ICMA, a separate input file named `init.txt` is read by the modified LAMMPS code; this file contains the following information: (i) total number of atoms in the system (line 2), (ii) number of modes that will be assigned to this computational node (line 4), and (iii) the frequency at which the modal contributions to heat flow will be calculated and recorded (line 6). Lines 1, 3, and 5 in `init.txt` are comments to the lines after them and will be ignored by the modified LAMMPS code.

In the current implementation of ICMA, the modal contributions are calculated and recorded from time step 1. This is important to note, since in MD simulations the structure is initially equilibrated using NVT or NPT ensembles; however, all the modal contributions should be calculated under the equilibrium NVE ensemble. Therefore, to post-process the obtained modal heat flux values and calculate cross-correlations, only the modal heat flux values corresponding to the equilibrium NVE stage should be considered, while other modal heat flux values from the equilibration phase should be neglected. The reason why

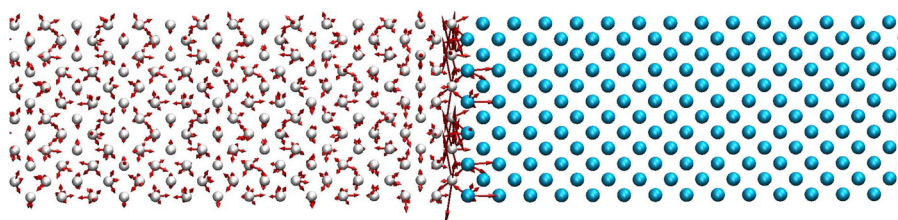


**FIG. 10.** Polarization vectors (red arrows) for one of the largely contributing modes in the range of 12-13 THz for the c-Si/c-Ge interface structure. White atoms and cyan atoms represent Si and Ge atoms, respectively.

the NVE ensemble should be used for modal analysis is because it does not disrupt the natural vibrations of atoms, which is critical in modal analysis methods that employ the fluctuation-dissipation theorem.<sup>63</sup>

The main challenge with implementing ICMA in LAMMPS is that at the time of writing this tutorial (22 August 2018), LAMMPS does not have a command to calculate the instantaneous interfacial heat flow between two groups of atoms. However, the interfacial heat flow values can still be calculated by modifying specific force routines<sup>72</sup> (i.e., interatomic potentials) that are called during the MD simulation. The main reason for choosing the force routine is that in calculating the instantaneous interfacial heat flow, we need access to the mutual forces ( $\mathbf{f}_{ij}$ ) that the interacting pair of atoms  $i$  and  $j$  exert on each other [see Eqs. (31) and (32)]. However, contrary to the total force on an atom, the individual mutual interactions between atoms are not stored in any variable in LAMMPS and can only be accessed inside the force routine. The example code provided in the [supplementary material](#) and explained below is taken from our modifications of the Tersoff interatomic potential used in the analysis of the Si/Ge interface; this example was chosen because it shows that ICMA is not restricted to pairwise interactions and can be applied to many-body potentials as well.

In addition to the forces ( $\mathbf{f}_{ij}$ ) used to calculate the modal velocity coordinates needed in ICMA formulations [Eqs. (31) and (32)], eigenvectors of vibration and atomic velocities are needed. Since the eigenvectors do not change in time, they are imported to the force routine once at the beginning of the simulation (see code block 4), while atomic velocities can be accessed globally in LAMMPS's architecture inside the force routine at each time step (see code block 3). As discussed in the GKMA section, the eigenvector values for different vibrational modes are stored in columns in a file (ev\_real.txt) that will be read by LAMMPS. For a system of  $N$  atoms, each column will include  $3N$  real numbers, since the  $\Gamma$ -point LD calculations (as explained in Sec. III A 1) will only result in real values for eigenvectors of vibration.<sup>37</sup>

For ease of programming, we have re-written Eq. (31), which was used to calculate modal contributions to heat flux, as follows:

$$Q_n = \dot{X}_n \left[ \sum_{i \in A} \sum_{j \in B} \left\{ \left( \frac{\partial \Phi_j}{\partial \mathbf{r}_i} \right) \cdot \left( \frac{1}{(m_i)^{1/2}} \mathbf{e}_{n,i} \right) + \left( \frac{-\partial \Phi_i}{\partial \mathbf{r}_j} \right) \cdot \left( \frac{1}{(m_j)^{1/2}} \mathbf{e}_{n,j} \right) \right\} \right]. \quad (42)$$

We then write  $F_n$  as

$$F_n = \sum_{i \in A} \sum_{j \in B} \left\{ \left( \frac{\partial \Phi_j}{\partial \mathbf{r}_i} \right) \cdot \left( \frac{1}{(m_i)^{1/2}} \mathbf{e}_{n,i} \right) + \left( \frac{-\partial \Phi_i}{\partial \mathbf{r}_j} \right) \cdot \left( \frac{1}{(m_j)^{1/2}} \mathbf{e}_{n,j} \right) \right\}. \quad (43)$$

Allowing Eq. (42) to be rewritten as

$$Q_n = \dot{X}_n F_n. \quad (44)$$

$\dot{X}_n$  is the modal velocity coordinate and is only a function of atomic velocities [see Eq. (7)]; thus, it can be determined as a one-block calculation in the beginning of the code at every time-step (see code block 5). Calculation of  $F_n$ , however, requires the values for mutual interatomic forces ( $\mathbf{f}_{ij}$ ) which are comprised of different types of interactions (pairwise, three body, four body, and so on) and thus should be calculated in different locations in the force routine code. For instance, in the case of the Tersoff potential, modifications to the code for capturing the pairwise and three body interactions are accomplished in code blocks 7 and 8, respectively.

Another point worth noting for ICMA calculations is that the simulation domain in a MD simulation can contain more than one instance of the specific interface under study. This might happen either because of periodic boundary conditions or because the structure under study is a superlattice.<sup>73,74</sup> In either case, since ICMA is formulated for an individual interface, interfacial heat flow calculations [e.g., Eq. (31)] should only be applied to one interface in the system. To study atomic interactions across a specific interface, one can assign different fictitious/placeholder atom types to the atoms at the interface of interest and only include the interactions between these atom types in the ICMA calculation. As an example, consider the interface between Si and Ge shown in Fig. 11(a). Because of the periodic boundary conditions in the system, Si and Ge atoms in this structure interact through two interfaces (one in the middle and one at the ends of the system). To account for the atomic interactions across only, e.g., the middle interface, we can consider two different atom types on each side of the structure, where as shown in Fig. 11(b), the interactions across the middle interface are now restricted between atom types 2 and 3. In our example code provided in the [supplementary material](#), if-statements have been utilized to only account for the interactions between atom types 2 and 3 (see blocks 7, 8 part 1 and 8 part 2).

Other modifications to the original Tersoff force routine in LAMMPS are

- A number of variables, such as  $F_n$ ,  $\dot{X}_n$ , eigenvectors of vibration, and the calculated modal heat fluxes, need to be accessed throughout the entire pair\_tersoff.cpp file. Thus, they are defined in the pair\_tersoff.h file (see code block 1).
- To access the number of time steps in LAMMPS, the header file update.h is added to the beginning of pair\_tersoff.cpp file (see code block 2).
- Atomic velocities and masses are accessed in code block 3.
- The files needed for reading the eigenvectors of vibration, reading the input init.txt, and recording the modal heat flux values are defined in code block 4.
- Modal velocity coordinates are calculated in code block 5.
- Atom types in the LAMMPS simulation can be accessed in code block 6.
- The pairwise interactions in the Tersoff potential are detected and used for calculating  $F_n$  in code block 7.
- In the Tersoff potential, the three body interactions are comprised of two parts. The atomic interactions in each

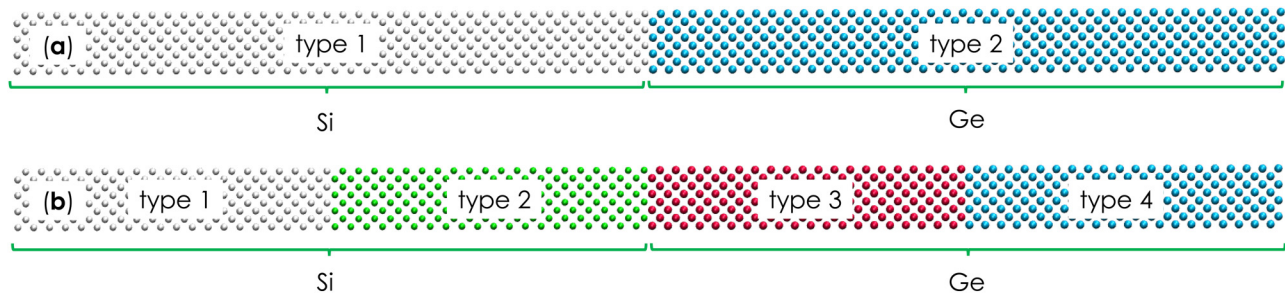


**FIG. 11.** Structure with interfaces between Si and Ge. (a) A generic MD simulation can be conducted by defining two atom types in the simulation. Then, if the boundary conditions are periodic, two interfaces will be present between atom types 1 and 2: one in the middle and one at the ends of the structure. (b) To only account for the atomic interactions across the middle interface, two additional atom types can be introduced, where now atom types 2 (Si) and 3 (Ge) interact only across the middle interface.

part are detected and used for calculating  $F_n$  in code block 8, part 1 and part 2.

- The calculated modal heat flux values are written to the output file in code block 9.

After the modal contributions are calculated, they can be quantum corrected following the same procedure as described for GKMA in Sec. II C. Additionally, in the case of hybrid potentials, in which two or more potentials are used to calculate the interaction between atoms in the system, the force routine for each interatomic potential can be modified to calculate and output the modal heat fluxes due to that potential. Then, in the post-processing phase, the calculated modal heat fluxes can be added together to obtain the total modal heat fluxes.

#### D. Sample case studies using ICMA

In this section, we discuss three important results from our prior ICMA studies. These results show the potential of ICMA in providing insight into the mechanisms of interfacial heat conduction, which might be challenging to capture using other existing models.

##### 1. The importance of anharmonicity

Harmonic interactions can only transfer energy elastically between modes of vibration that have equal frequencies.<sup>75,76</sup> Therefore, any contribution to interfacial heat transfer by a mode of vibration that has a frequency higher than the maximum frequency of vibration belonging to the bulk of the heavier/weaker side of the interface that has a lower maximum vibration frequency (i.e.,  $\omega_{max,B}$ ) can only be attributed to the anharmonic interactions. Some reports have reasoned that inelastic interactions across interfaces play a critical role in interfacial heat transfer;<sup>77,78</sup> however, others have questioned the significance of anharmonic effects.<sup>79</sup> Nonetheless, the ICMA technique can determine one definitive portion of the anharmonic contributions to TIC, via the contributions above  $\omega_{max,B}$ . This provides one way to assess

the significance of anharmonicity in interfacial heat conduction, but it is not complete, since anharmonic contributions could also be important below  $\omega_{max,B}$ . However, a second approach to distinguishing the anharmonic vs. harmonic contributions is to examine the net TIC contribution due to the auto and cross correlations. Elastic/harmonic contributions are restricted to appearing in the auto-correlations, and therefore the cross-correlations can also be attributed to anharmonic effects. However, there could still be an anharmonic contribution embedded inside the autocorrelations as well, and thus it is not clear at present how to conclusively and completely separate out the anharmonic vs. harmonic contributions using ICMA.

Using ICMA, Gordiz and Henry<sup>28-30</sup> investigated the modal contributions and anharmonic interactions across eight different interfaces between crystalline, amorphous, and alloyed materials. Example interfaces labeled (1-6) consisted of all the possible combinations between dissimilar materials made of crystalline (c-) and amorphous (a-) Si and Ge materials.<sup>29</sup> Interface (7) consisted of a c-Si/a-SiO<sub>2</sub><sup>30</sup> interface, and example (8) was an InP/In<sub>0.53</sub>Ga<sub>0.47</sub>As<sup>28</sup> interface. The TIC accumulation results are shown in Fig. 12. All the contributions to the TIC above  $\omega_{max,B}$  are attributed to the anharmonic interactions. For instance, in the InP/In<sub>0.53</sub>Ga<sub>0.47</sub>As interface, there is a phononic bandgap in the InP structure (see Fig. 13), and therefore there is no overlap of vibrational frequencies between the two, i.e., between 5.7 and 10 THz. This is because bulk InP has no modes in this frequency regime and In<sub>0.53</sub>Ga<sub>0.47</sub>As has a maximum frequency just below 10 THz, and therefore the modes in InP above 10 THz have no corresponding match in In<sub>0.53</sub>Ga<sub>0.47</sub>As. Therefore, all the contributions to the TIC for InP/InGaAs interface by frequencies higher than 5.7 THz can be attributed to anharmonic interactions. Figure 12 clearly shows that except for c-Si/a-Si and c-Ge/a-Ge interfaces, anharmonicity has at least a 19% contribution to the TIC across all the other interfaces, which supports the idea that anharmonicity plays an important role in TIC. If one were to separately compute the cross-correlation contributions, it is

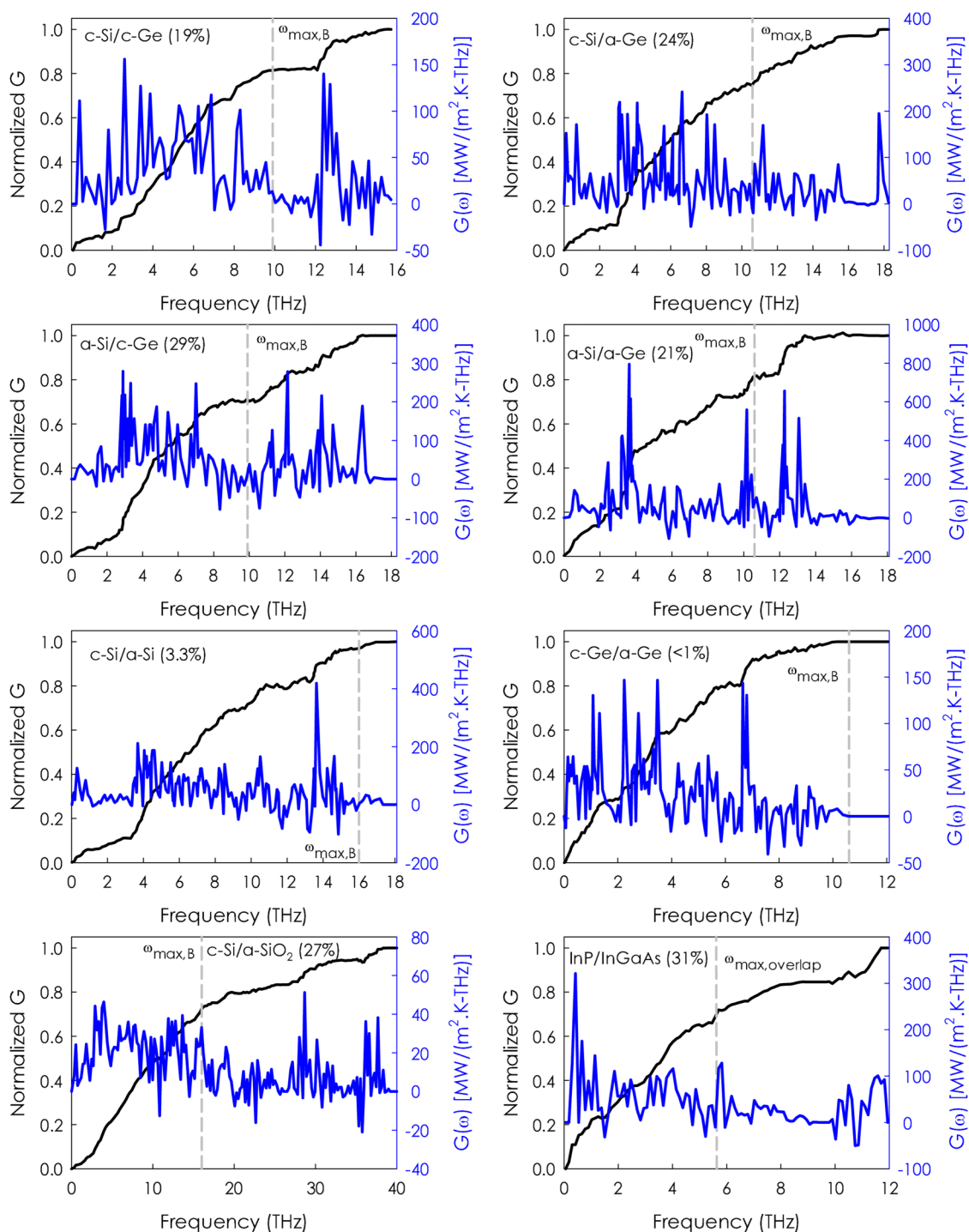


**FIG. 12.** TIC accumulation functions (black curves for left y-axes) and frequency dependent TIC (blue curves for right y-axes) for eight different interfaces. Anharmonic contributions are present at frequencies higher than the maximum frequency of vibration at the bulk of the heavier/weaker side of the interface (denoted here by  $\omega_{\max,B}$ ). For InP/InGaAs interface, anharmonic contributions are present at frequencies above the beginning of the InP bandgap (denoted here by  $\omega_{\max,overlap}$ ) above which no overlap of frequencies exists between the two sides (see Fig. 13). The percentages given as insets on each figure panel denote what fraction of the TIC is association with anharmonicity. The presented modal contributions in this figure are not quantum corrected.

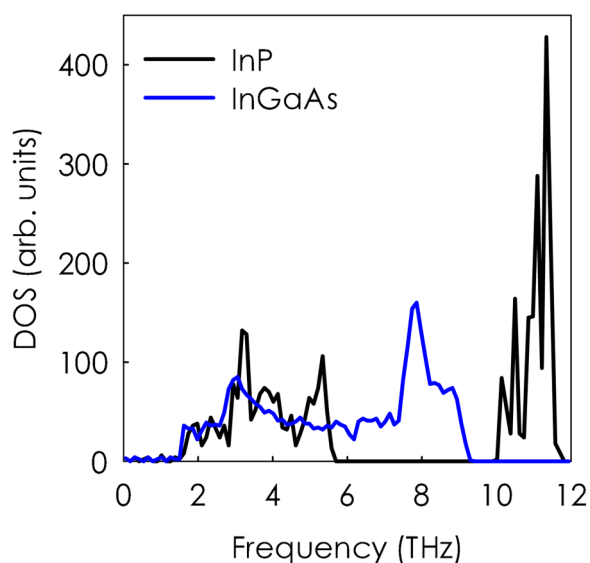


**FIG. 13.** DOS for the bulk InP and InGaAs structures. Above 5.7 THz, no frequency overlap exists.

likely that the total anharmonic contributions could be even larger. Recently, several other approaches have also been proposed in the literature<sup>24-26</sup> that calculates the anharmonic spectral contributions to TIC. These techniques are mainly based on NEMD simulations, and their obtained modal analysis is usually presented as frequency dependent contributions to TIC. To facilitate the comparison between the ICMA approach and these techniques,<sup>24-26</sup> the frequency dependent contributions to TIC are also included in Fig. 12 for the considered interfaces.

## 2. The significant role of interfacial modes

Using ICMA, examining the heat conduction at c-Si/c-Ge interfaces in more detail reveals that a group of modes around 12-13 THz contribute more than 15% to the TIC.<sup>27</sup> Examining the DOS of vibrational modes in this interfacial system indicates that the region of 12-13 THz vibrations does not correspond to a region with considerable population of modes, which one might think to be the reason for >15% contribution to the TIC from a small frequency range. This large contribution to TIC by this narrow frequency range has also been reported in other studies<sup>26,30</sup> that have used other computational techniques. However, using ICMA, it is not only possible

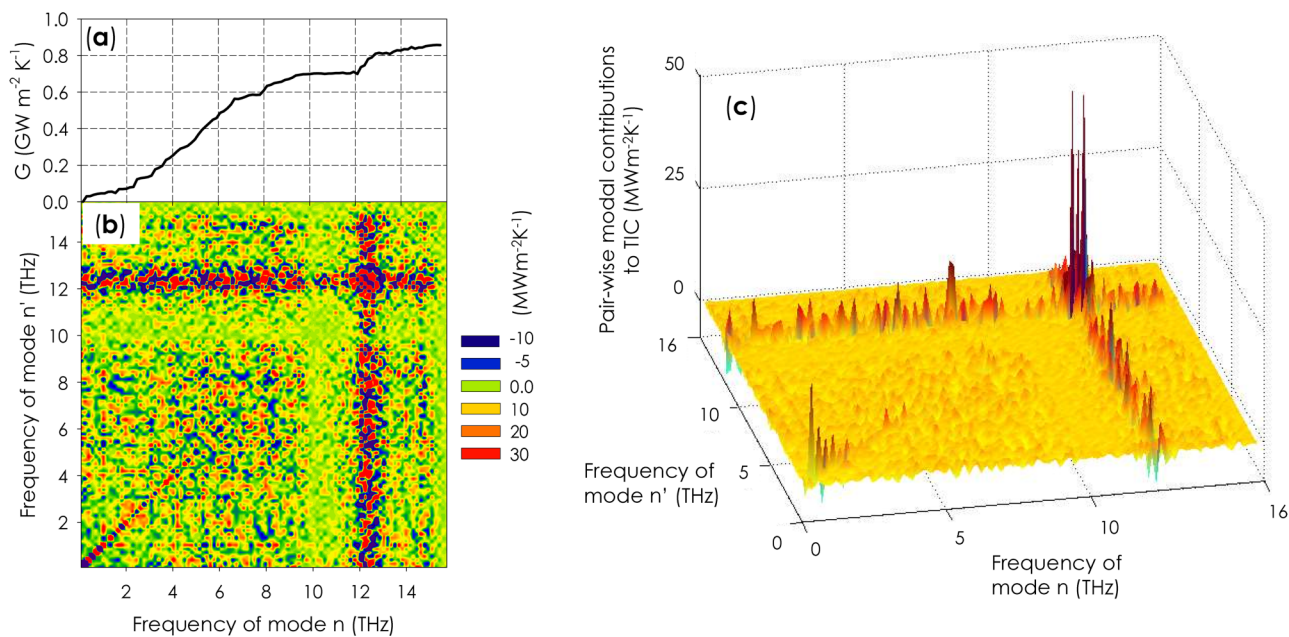


**FIG. 14.** Modal contributions to TIC for Si/Ge interface at  $T = 300$  K.<sup>27</sup> (a) TIC accumulation function, (b) 2D map, and (c) 3D perspective depiction of the data in (b) showing the magnitudes of the correlations as elevations above the plane of two frequency axes. The values presented on the 2D and 3D maps have units of  $(MW m^{-2} K^{-1})$ . Inelastic interactions occur between the modes with frequencies 12-13 THz and all the other modes in the system. Although panel (a) shows that interfacial modes in the frequency range of 12-13 THz contribute almost 15% to the TIC, the summation of the contribution of interfacial modes on the correlation maps of (b) and (c) shows that when their affects/correlations with other modes are also included they are, in total, responsible for more than 26% of the total TIC. The presented modal contributions in this figure are not quantum corrected.

to determine the exact number of these contributing modes, but also we could determine their eigen vectors to better understand how they behave. By investigating all the eigen modes present in the range of 12–13 THz, it was determined that all of this large contribution to TIC arises from only a few modes occupying approximately 0.3% of the total population of modes. The polarization vectors for one of these modes are shown in Fig. 10. It can be seen that these largely contributing modes have a large degree of their energy localized around the interface; however, they also have vibrations on the bulk of the Si side. As Fig. 14 shows, these eigen-vectors of vibrations have allowed these modes of vibration with frequencies around 12–13 THz to strongly couple to all the other modes of vibration in the system and transfer their energy across the interface, which is reflected on the strong cross-correlation band around the 12–13 THz region.

In the second half of this tutorial, we formulated the ICMA formalism which allows one to calculate the modal contributions to the TIC from MD simulations. The approach is based on the modal decomposition of the instantaneous heat flow across an interface, which can be implemented in either EMD or NEMD simulations. Several results from prior studies of interfacial heat conduction using ICMA were examined, and some of the insights obtained from ICMA such as the large contribution of non-propagating localized modes to the TIC were discussed. Many additional comparative studies to better understand the effects of temperature, anharmonicity, inter-diffusion, roughness, imperfections, dislocations, stress, changes in crystal structure, etc. are needed. The ICMA formalism serves as an important step forward, which has now provided a new lens for studying such effects. Coupled with more accurate experimental techniques for TIC measurements, such as transducer-less Time-domain thermoreflectance (TL-TDTR)<sup>81</sup> for validating the ICMA predictions, ICMA has the potential to provide insights on how to rationally design and select materials for applications involving heat flow across interfaces.

#### IV. SUMMARY

In this tutorial, we have presented the formalism, implementation, and application of GKMA and ICMA to predict the thermal conductivity and TIC, respectively. Both methods calculate the contribution of phonons to the thermal transport using a unified perspective based on the time correlation of the heat current, which is fundamentally different compared to the more widely accepted paradigm based on scattering. The advantage of these methods over the existing PGM based methods is that they can predict the transport in crystalline materials with any level of defects, up through fully amorphous solids, dilute to fully random alloys, molecules, nanostructures, and across interfaces involving any of these material classes. We reviewed the calculation of TC and TIC of some bulk solids and interfaces to demonstrate the basic idea of the GKMA and ICMA methods as well as to highlight the connection between the heat current correlations and the transport properties.

#### SUPPLEMENTARY MATERIAL

See the [supplementary material](#) for the necessary codes and their respective explanations for running GKMA and ICMA calculations.

#### REFERENCES

- <sup>1</sup>G. Chen, *Nanoscale Energy Transport and Conversion: A Parallel Treatment of Electrons, Molecules, Phonons, and Photons* (Oxford University Press, 2005).
- <sup>2</sup>R. E. Peierls, *Quantum theory of solids* (Clarendon Press, 1996).
- <sup>3</sup>K. Gordiz and A. Henry, "Phonon transport at interfaces: Determining the correct modes of vibration," *J. Appl. Phys.* **119**, 015101 (2016).
- <sup>4</sup>W. Lv and A. Henry, "Direct calculation of modal contributions to thermal conductivity via Green-Kubo modal analysis," *New J. Phys.* **18**, 013028 (2016).
- <sup>5</sup>W. Lv and A. Henry, "Phonon transport in amorphous carbon using Green-Kubo modal analysis," *Appl. Phys. Lett.* **108**, 181905 (2016).
- <sup>6</sup>W. Lv and A. Henry, "Non-negligible contributions to thermal conductivity from localized modes in amorphous silicon dioxide," *Sci. Rep.* **6**, 35720 (2016).
- <sup>7</sup>W. Lv and A. Henry, "Examining the validity of the phonon gas model in amorphous materials," *Sci. Rep.* **6**, 37675 (2016).
- <sup>8</sup>G. P. Srivastava, *The Physics of Phonons* (CRC Press, 1990).
- <sup>9</sup>J. M. Ziman, *Electrons and Phonons: The Theory of Transport Phenomena in Solids* (Oxford University Press, 2001).
- <sup>10</sup>B. Abeles, "Lattice thermal conductivity of disordered semiconductor alloys at high temperatures," *Phys. Rev.* **131**, 1906–1911 (1963).
- <sup>11</sup>D. G. Cahill et al., "Nanoscale thermal transport. II. 2003–2012," *Appl. Phys. Rev.* **1**, 011305 (2014).
- <sup>12</sup>K. Esfarjani, J. Garg, and G. Chen, "Modeling heat conduction from first principles," *Annu. Rev. Heat Transf.* **17**, 9–47 (2014).
- <sup>13</sup>T. Feng and X. Ruan, "Prediction of spectral phonon mean free path and thermal conductivity with applications to thermoelectrics and thermal management: A review," *J. Nanomater.* **2014**, 206370 (2014).
- <sup>14</sup>L. Lindsay, D. Broido, and T. Reinecke, "Ab initio thermal transport in compound semiconductors," *Phys. Rev. B* **87**, 165201 (2013).
- <sup>15</sup>T. Tadano, Y. Gohda, and S. Tsuneyuki, "Anharmonic force constants extracted from first-principles molecular dynamics: Applications to heat transfer simulations," *J. Phys. Condens. Matter* **26**, 225402 (2014).
- <sup>16</sup>T. Tadano and S. Tsuneyuki, "Self-consistent phonon calculations of lattice dynamical properties in cubic SrTiO<sub>3</sub> with first-principles anharmonic force constants," *Phys. Rev. B* **92**, 054301 (2015).
- <sup>17</sup>X. Wang and B. Huang, "Computational study of in-plane phonon transport in Si thin films," *Sci. Rep.* **4**, 6399 (2014).
- <sup>18</sup>J. Zhou, B. Liao, and G. Chen, "First-principles calculations of thermal, electrical, and thermoelectric transport properties of semiconductors," *Semicond. Sci. Technol.* **31**, 043001 (2016).
- <sup>19</sup>H. R. Seyf et al., "Rethinking phonons: The issue of disorder," *NPJ Comput. Mater.* **3**, 49 (2017).
- <sup>20</sup>K. Sääskilähti, J. Oksanen, S. Volz, and J. Tulkki, "Frequency-dependent phonon mean free path in carbon nanotubes from nonequilibrium molecular dynamics," *Phys. Rev. B* **91**, 115426 (2015).
- <sup>21</sup>Y. Zhou and M. Hu, "Erratum: Quantitatively analyzing phonon spectral contribution of thermal conductivity based on nonequilibrium molecular dynamics simulations. II. From time Fourier transform [Phys. Rev. B **92**, 195205 (2015)]," *Phys. Rev. B* **93**, 039901 (2016).
- <sup>22</sup>Y. Zhou, X. Zhang, and M. Hu, "Quantitatively analyzing phonon spectral contribution of thermal conductivity based on nonequilibrium molecular dynamics simulations. I. From space Fourier transform," *Phys. Rev. B* **92**, 195204 (2015).
- <sup>23</sup>K. Gordiz and A. Henry, "A formalism for calculating the modal contributions to thermal interface conductance," *New J. Phys.* **17**, 103002 (2015).

- <sup>24</sup>Y. Chalopin and S. Volz, "A microscopic formulation of the phonon transmission at the nanoscale," *Appl. Phys. Lett.* **103**, 051602 (2013).
- <sup>25</sup>K. Säskilähti, J. Oksanen, J. Tulkki, and S. Volz, "Role of anharmonic phonon scattering in the spectrally decomposed thermal conductance at planar interfaces," *Phys. Rev. B* **90**, 134312 (2014).
- <sup>26</sup>Y. Zhou and M. Hu, "Full quantification of frequency-dependent interfacial thermal conductance contributed by two- and three-phonon scattering processes from nonequilibrium molecular dynamics simulations," *Phys. Rev. B* **95**, 115313 (2017).
- <sup>27</sup>K. Gordiz and A. Henry, "Phonon transport at crystalline Si/Ge interfaces: The role of interfacial modes of vibration," *Sci. Rep.* **6** (2016).
- <sup>28</sup>K. Gordiz and A. Henry, "Interface conductance modal analysis of lattice matched InGaAs/InP," *Appl. Phys. Lett.* **108**, 181606 (2016).
- <sup>29</sup>K. Gordiz and A. Henry, "Phonon transport at interfaces between different phases of silicon and germanium," *J. Appl. Phys.* **121**, 025102 (2017).
- <sup>30</sup>K. Gordiz, M. G. Muraleedharan, and A. Henry, "Modal analysis of heat transfer across crystalline Si and amorphous SiO<sub>2</sub> interface," preprint [arXiv:1807.06633](https://arxiv.org/abs/1807.06633) (2018).
- <sup>31</sup>K. Gordiz, D. J. Singh, and A. Henry, "Ensemble averaging vs. time averaging in molecular dynamics simulations of thermal conductivity," *J. Appl. Phys.* **117**, 045104 (2015).
- <sup>32</sup>A. Henry and G. Chen, "High thermal conductivity of single polyethylene chains using molecular dynamics simulations," *Phys. Rev. Lett.* **101**, 235502 (2008).
- <sup>33</sup>A. Henry and G. Chen, "Anomalous heat conduction in polyethylene chains: Theory and molecular dynamics simulations," *Phys. Rev. B* **79**, 144305 (2009).
- <sup>34</sup>A. S. Henry and G. Chen, "Spectral phonon transport properties of silicon based on molecular dynamics simulations and lattice dynamics," *J. Comput. Theor. Nanosci.* **5**, 141–152 (2008).
- <sup>35</sup>M. G. Muraleedharan et al., "Thermal interface conductance between aluminum and aluminum oxide: A rigorous test of atomistic level theories," preprint [arXiv:1807.06631](https://arxiv.org/abs/1807.06631) (2018).
- <sup>36</sup>R. J. Hardy, "Energy-flux operator for a lattice," *Phys. Rev.* **132**, 168 (1963).
- <sup>37</sup>M. T. Dove, *Introduction to Lattice Dynamics* (Cambridge University press, 1993), Vol. 4.
- <sup>38</sup>H. R. Seyf, W. Lv, A. Rohskopf, and A. Henry, "The importance of phonons with negative phase quotient in disordered solids," *Sci. Rep.* **8**, 2627 (2018).
- <sup>39</sup>J. Turney, A. McGaughey, and C. Amon, "Assessing the applicability of quantum corrections to classical thermal conductivity predictions," *Phys. Rev. B* **79**, 224305 (2009).
- <sup>40</sup>J. Larkin, J. Turney, A. Massicotte, C. Amon, and A. McGaughey, "Comparison and evaluation of spectral energy methods for predicting phonon properties," *J. Comput. Theor. Nanosci.* **11**, 249–256 (2014).
- <sup>41</sup>S. Plimpton, "Fast parallel algorithms for short-range molecular dynamics," *J. Comput. Phys.* **117**, 1–19 (1995).
- <sup>42</sup>P. F. Dubois, K. Hinsen, and J. Hugunin, "Numerical python," *Comput. Phys.* **10**, 262–267 (1996).
- <sup>43</sup>J. D. Gale and A. L. Rohl, "The general utility lattice program (GULP)," *Mol. Simulat.* **29**, 291–341 (2003).
- <sup>44</sup>A. Togo and I. Tanaka, "First principles phonon calculations in materials science," *Scr. Mater.* **108**, 1–5 (2015).
- <sup>45</sup>Z. Tian, K. Esfarjani, J. Shiomi, A. S. Henry, and G. Chen, "On the importance of optical phonons to thermal conductivity in nanostructures," *Appl. Phys. Lett.* **99**, 053122 (2011).
- <sup>46</sup>J. M. Haile, "Molecular dynamics simulation," *Elementary Methods* **1**, 38 (1992).
- <sup>47</sup>A. McGaughey, M. Hussein, E. Landry, M. Kaviani, and G. Hulbert, "Phonon band structure and thermal transport correlation in a layered diatomic crystal," *Phys. Rev. B* **74**, 104304 (2006).
- <sup>48</sup>A. McGaughey and M. Kaviani, "Observation and description of phonon interactions in molecular dynamics simulations," *Phys. Rev. B* **71**, 184305 (2005).
- <sup>49</sup>J. Tersoff, "New empirical approach for the structure and energy of covalent systems," *Phys. Rev. B* **37**, 6991 (1988).
- <sup>50</sup>D. Broido, M. Malorny, G. Birner, N. Mingo, and D. Stewart, "Intrinsic lattice thermal conductivity of semiconductors from first principles," *Appl. Phys. Lett.* **91**, 231922 (2007).
- <sup>51</sup>K. Esfarjani, G. Chen, and H. T. Stokes, "Heat transport in silicon from first-principles calculations," *Phys. Rev. B* **84**, 085204 (2011).
- <sup>52</sup>M. Z. Bazant, E. Kaxiras, and J. F. Justo, "Environment-dependent interatomic potential for bulk silicon," *Phys. Rev. B* **56**, 8542 (1997).
- <sup>53</sup>P. B. Allen and J. L. Feldman, "Thermal conductivity of disordered harmonic solids," *Phys. Rev. B* **48**, 12581 (1993).
- <sup>54</sup>P. B. Allen, J. L. Feldman, J. Fabian, and F. Wooten, "Diffusons, locons and propagons: Character of atomic vibrations in amorphous Si," *Philos. Mag. B* **79**, 1715–1731 (1999).
- <sup>55</sup>R. Biswas, A. Bouchard, W. Kamitakahara, G. Grest, and C. Soukoulis, "Vibrational localization in amorphous silicon," *Phys. Rev. Lett.* **60**, 2280 (1988).
- <sup>56</sup>H. R. Seyf and A. Henry, "A method for distinguishing between propagons, diffusons, and locons," *J. Appl. Phys.* **120**, 025101 (2016).
- <sup>57</sup>W. Lv, R. M. Winters, F. DeAngelis, G. Weinberg, and A. Henry, "Understanding divergent thermal conductivity in single polythiophene chains using Green-Kubo modal analysis and sonification," *J. Phys. Chem. A* **121**, 5586–5596 (2017).
- <sup>58</sup>K. Gordiz, *Modal Decomposition of Thermal Conductance* (Georgia Institute of Technology, 2017).
- <sup>59</sup>G. Domingues, S. Volz, K. Joulain, and J.-J. Greffet, "Heat transfer between two nanoparticles through near field interaction," *Phys. Rev. Lett.* **94**, 085901 (2005).
- <sup>60</sup>L. Puech, G. Bonfait, and B. Castaing, "Mobility of the 3He solid-liquid interface: Experiment and theory," *J. Low Temp. Phys.* **62**, 315–327 (1986).
- <sup>61</sup>Y. Chalopin, K. Esfarjani, A. Henry, S. Volz, and G. Chen, "Thermal interface conductance in Si/Ge superlattices by equilibrium molecular dynamics," *Phys. Rev. B* **85**, 195302 (2012).
- <sup>62</sup>Z.-Y. Ong and E. Pop, "Frequency and polarization dependence of thermal coupling between carbon nanotubes and SiO<sub>2</sub>," *J. Appl. Phys.* **108**, 103502 (2010).
- <sup>63</sup>R. Kubo, "The fluctuation-dissipation theorem," *Rep. Prog. Phys.* **29**, 255 (1966).
- <sup>64</sup>P. K. Schelling, S. R. Phillpot, and P. Keblinski, "Phonon wave-packet dynamics at semiconductor interfaces by molecular-dynamics simulation," *Appl. Phys. Lett.* **80**, 2484–2486 (2002).
- <sup>65</sup>N. A. Roberts and D. Walker, "Phonon wave-packet simulations of Ar/Kr interfaces for thermal rectification," *J. Appl. Phys.* **108**, 123515 (2010).
- <sup>66</sup>K. Gordiz and S. M. V. Allaei, "Thermal rectification in pristine-hydrogenated carbon nanotube junction: A molecular dynamics study," *J. Appl. Phys.* **115**, 163512 (2014).
- <sup>67</sup>X. Wu and T. Luo, "The importance of anharmonicity in thermal transport across solid-solid interfaces," *J. Appl. Phys.* **115**, 014901 (2014).
- <sup>68</sup>A. Rajabpour, S. V. Allaei, and F. Kowsary, "Interface thermal resistance and thermal rectification in hybrid graphene-graphane nanoribbons: A nonequilibrium molecular dynamics study," *Appl. Phys. Lett.* **99**, 051917 (2011).
- <sup>69</sup>M. Hu, P. Keblinski, and P. K. Schelling, "Kapitza conductance of silicon-amorphous polyethylene interfaces by molecular dynamics simulations," *Phys. Rev. B* **79**, 104305 (2009).
- <sup>70</sup>P. Kapitza, "The study of heat transfer in helium II," *J. Phys. (USSR)* **4**, 181–210 (1941).
- <sup>71</sup>E. Landry and A. McGaughey, "Thermal boundary resistance predictions from molecular dynamics simulations and theoretical calculations," *Phys. Rev. B* **80**, 165304 (2009).
- <sup>72</sup>A. Rohskopf, H. R. Seyf, K. Gordiz, T. Tadano, and A. Henry, "Empirical interatomic potentials optimized for phonon properties," *NPJ Comput. Mater.* **3**, 27 (2017).
- <sup>73</sup>A. Giri, J. L. Braun, and P. E. Hopkins, "Effect of crystalline/amorphous interfaces on thermal transport across confined thin films and superlattices," *J. Appl. Phys.* **119**, 235305 (2016).
- <sup>74</sup>A. Giri, P. E. Hopkins, J. G. Wessel, and J. C. Duda, "Kapitza resistance and the thermal conductivity of amorphous superlattices," *J. Appl. Phys.* **118**, 165303 (2015).

- <sup>75</sup>E. R. Pike and P. C. Sabatier, *Scattering, Two-Volume Set: Scattering and Inverse Scattering in Pure and Applied Science* (Academic Press, 2001).
- <sup>76</sup>V. V. Varadan, *Acoustic, Electromagnetic and Elastic Wave Scattering-Focus on the T-Matrix Approach* (Pergamon, 1980), pp. 33–59.
- <sup>77</sup>T. S. English *et al.*, “Enhancing and tuning phonon transport at vibrationally mismatched solid-solid interfaces,” *Phys. Rev. B* **85**, 035438 (2012).
- <sup>78</sup>R. J. Stevens, L. V. Zhigilei, and P. M. Norris, “Effects of temperature and disorder on thermal boundary conductance at solid-solid interfaces: Nonequilibrium molecular dynamics simulations,” *Int. J. Heat Mass Transf.* **50**, 3977–3989 (2007).
- <sup>79</sup>W. Zhang, T. Fisher, and N. Mingo, “The atomistic Green’s function method: An efficient simulation approach for nanoscale phonon transport,” *Numer. Heat Trans. B Fundam.* **51**, 333–349 (2007).
- <sup>80</sup>T. Murakami, T. Hori, T. Shiga, and J. Shiomi, “Probing and tuning inelastic phonon conductance across finite-thickness interface,” *Appl. Phys. Express* **7**, 121801 (2014).
- <sup>81</sup>L. Wang, R. Cheaito, J. Braun, A. Giri, and P. Hopkins, “Thermal conductivity measurements of non-metals via combined time-and frequency-domain thermoreflectance without a metal film transducer,” *Rev. Sci. Instrum.* **87**, 094902 (2016).